THE HEAVY QUARK-ANTIQUARK POTENTIAL

AND ITS RELATIVES AT SHORT DISTANCES

ANTONIO PINEDA

(IFAE, UAB)

Hydrogen atom

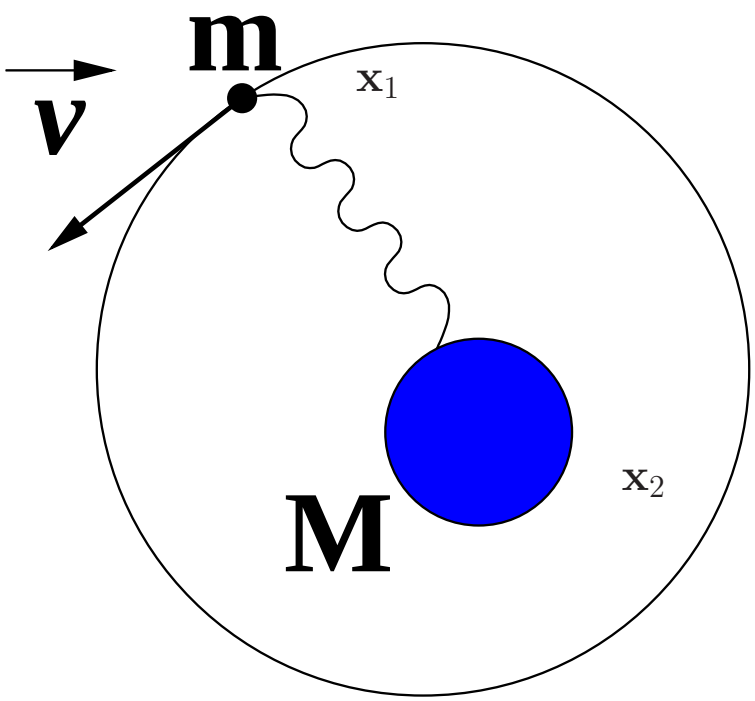

$$V(r) = -\frac{Z_1 Z_2 \alpha}{r}$$

$$v \sim \alpha \ll 1$$

$$\mathbf{x} = \mathbf{x}_1 - \mathbf{x}_2 \qquad \mathbf{X} = \frac{m}{m+M}\mathbf{x}_1 + \frac{M}{m+M}\mathbf{x}_2$$

Scales: m (hard), $m\alpha$ (soft), $m\alpha^2$ (ultrasoft), ... $\rightarrow$ Effective Field Theories.

Potentials appear in heavy quarkonium ($v \ll 1$).

NR Effective Field Theories

Our aim is to provide a systematic method to deal with NR bound state systems. We will introduce a hierarchy of EFTs when sequentially integrating out each scale (only one scale in each step, strong simplification).

QCD

↓ Integrating out the hard scale (m)

NRQCD — Caswell, Lepage; Bodwin, Braaten, Lepage

↓ Integrating out the soft scale (mv)

pNRQCD — Pineda, Soto; Brambilla, Pineda, Soto, Vairo

$$\left.\begin{array}{l}\left(i\partial_0 - \dfrac{\mathbf{p}^2}{2m} - V_0(r)\right)\Phi(\mathbf{r}) = 0 \\ +\text{corrections to the potential} \\ +\text{interaction with other low} \\ \quad \text{energy degrees of freedom}\end{array}\right\} \text{potential NRQCD} \qquad E \sim mv^2$$

In the perturbative case the starting point is $V_0 = -C_f \dfrac{\alpha}{r}$.

pNRQCD: the scale mv

The integration of the mv scale gives rise to potential terms. The Lagrangian is local in time but not in space.

Playing with the scales:

1) $mv \sim \Lambda_{QCD}$

2) $mv \gg \Lambda_{QCD}$

Loosely speaking, when to trust the perturbative calculation and the size of NP corrections.

$mv \gg \Lambda_{QCD}$ ($\Upsilon(1S)$, t-$\bar{t}$, b-$\bar{b}$ sum rules)

$$\begin{aligned}
\mathcal{L}_{pNRQCD} &= \mathrm{Tr}\{S^\dagger \left(i\partial_0 - V_s^{(0)}(\mathbf{x})\right) S + O^\dagger \left(iD_0 - V_o^{(0)}(\mathbf{x})\right) O\} \\
&+ gV_A(\mathbf{x})\mathrm{Tr}\left\{O^\dagger \mathbf{x}\cdot\mathbf{E}\, S + S^\dagger \mathbf{x}\cdot\mathbf{E}\, O\right\} + g\frac{V_B(\mathbf{x})}{2}\mathrm{Tr}\left\{O^\dagger \mathbf{x}\cdot\mathbf{E}\, O + O^\dagger O \mathbf{x}\cdot\mathbf{E}\right\} \\
&- \mathrm{Tr}\{S^\dagger \left(\frac{\mathbf{p}^2}{m} + \sum_n \frac{V_s^{(n)}(\mathbf{x})}{m^n}\right) S - O^\dagger \left(\frac{\mathbf{p}^2}{m} + \sum_n \frac{V_o^{(n)}(\mathbf{x})}{m^n}\right) O\} + \text{ultrasoft gluons},
\end{aligned}$$

Interpolating fields:

$$Q_2^\dagger(\mathbf{x}_2,t)\phi(\mathbf{x}_2,\mathbf{x}_1;t)Q_1(\mathbf{x}_1,t) = Z_s^{1/2}(\mathbf{x})S(\mathbf{X},\mathbf{x},t)$$

$$Q_2^\dagger(x_2)\phi(\mathbf{x}_2,\mathbf{X};t)T^a\phi(\mathbf{X},\mathbf{x}_1;t)Q_1(x_1) = Z_o^{1/2}(\mathbf{x})O^a(\mathbf{X},\mathbf{x},t)$$

$$V = \sum_i c_i(m/\mu)\tilde{V}_i(\mu r; r)$$

$c_i(m/\mu) \longrightarrow$ NRQCD matching coefficients, computable in perturbation theory in $\alpha_s(m)$
$\tilde{V}_i(\mu r; r)$, computable in perturbation theory in $\alpha_s(1/r)$

$mv \sim \Lambda_{QCD}$ (b-$\bar{b}$,c-$\bar{c}$)

Degrees of freedom (?): (trial-error, mass gap, we do not see hybrids)
Static NRQCD: $D_{\infty h}$ (substituting parity by CP).

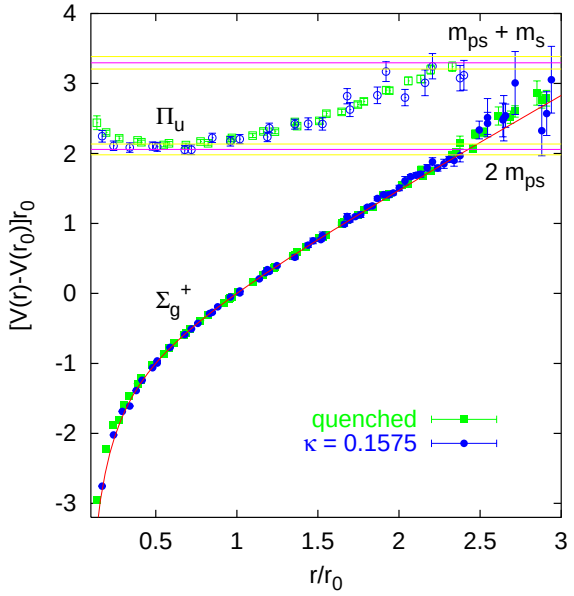

Figure 1: $r_0 \simeq 0.5$ *fm. From SESAM, hep-lat/0003012.*

Matching scale $\Lambda \ll \Lambda_{QCD}$. Coloured-like degrees of freedom decouple. Mass gap of hybrids and glueballs of $O(\Lambda_{QCD}) \gg mv^2$.

S, O and soft gluons $\longrightarrow$ S

- Pure QCD (no light fermions): the singlet (S)
- QCD: singlet plus pions (non-potential effects).

$mv \sim \Lambda_{QCD}$ $(b\text{-}\bar{b}, c\text{-}\bar{c})$

$$\mathcal{L}_{pNRQCD} = \mathrm{Tr}\{S^\dagger \left(i\partial_0 - V_s^{(0)}(\mathbf{x})\right) S - \mathrm{Tr}\{S^\dagger \left(\frac{\mathbf{p}^2}{m} + \sum_n \frac{V_s^{(n)}(\mathbf{x})}{m^n}\right) S\},$$

$$\begin{aligned} V^{(2,0)} \;=\; & \frac{1}{2}\left\{\mathbf{p}_1^2, V_{\mathbf{p}^2}^{(2,0)}(r)\right\} + \frac{V_{\mathbf{L}^2}^{(2,0)}(r)}{r^2}\mathbf{L}_1^2 + V_r^{(2,0)}(r) \quad \text{(SI)} \\ & + V_{LS}^{(2,0)}(r)\mathbf{L}_1\cdot\mathbf{S}_1 \quad \text{(SD)} \end{aligned}$$

$$\begin{aligned} V^{(1,1)} \;=\; & -\frac{1}{2}\left\{\mathbf{p}_1\cdot\mathbf{p}_2, V_{\mathbf{p}^2}^{(1,1)}(r)\right\} - \frac{V_{\mathbf{L}^2}^{(1,1)}(r)}{2r^2}(\mathbf{L}_1\cdot\mathbf{L}_2 + \mathbf{L}_2\cdot\mathbf{L}_1) + V_r^{(1,1)}(r) \quad \text{(SI)} \\ & + V_{L_1S_2}^{(1,1)}(r)\mathbf{L}_1\cdot\mathbf{S}_2 - V_{L_2S_1}^{(1,1)}(r)\mathbf{L}_2\cdot\mathbf{S}_1 + V_{S^2}^{(1,1)}(r)\mathbf{S}_1\cdot\mathbf{S}_2 + V_{\mathbf{S}_{12}}^{(1,1)}(r)\mathbf{S}_{12}(\hat{\mathbf{r}}) \quad \text{(SD)} \end{aligned}$$

$V^{(0)}$: Wilson, Susskind

$V_{LS}^{(2,0)}$, $V_{S^2}^{(1,1)}$, $V_{S_{12}}^{(1,1)}$: Eichten, Feinberg; Peskin; Gromes; Cheng, Kuang, Oakes; Barchielli, Montaldi, Prosperi; Barchielli, Brambilla, Prosperi; Szczepaniak, Swanson; Vairo, Pineda

$V_{L_1S_2}^{(1,1)}$: Vairo, Pineda; Szczepaniak, Swanson; Eichten, Feinberg

$V_{\mathbf{p}^2}^{(2,0)}$, $V_{\mathbf{L}^2}^{(2,0)}$, $V_{\mathbf{p}^2}^{(1,1)}$, $V_{\mathbf{L}^2}^{(1,1)}$: Barchielli, Montaldi, Prosperi; Barchielli, Brambilla, Prosperi; Vairo, Pineda

$V^{(1,1)}$: Brambilla, Soto, Vairo, Pineda

$V_r^{(2,0)}$, $V_r^{(1,1)}$: Vairo, Pineda

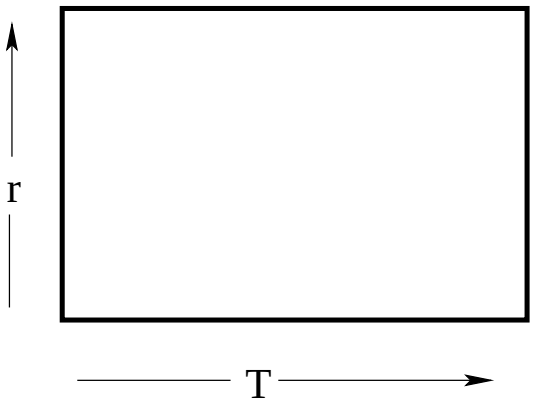

Figure 2: *Graphic representation of the static Wilson loop. We adopt the convention that the time propagates from the left to the right. Therefore, horizontal lines correspond to the quark trajectories and the vertical lines to the Schwinger strings.*

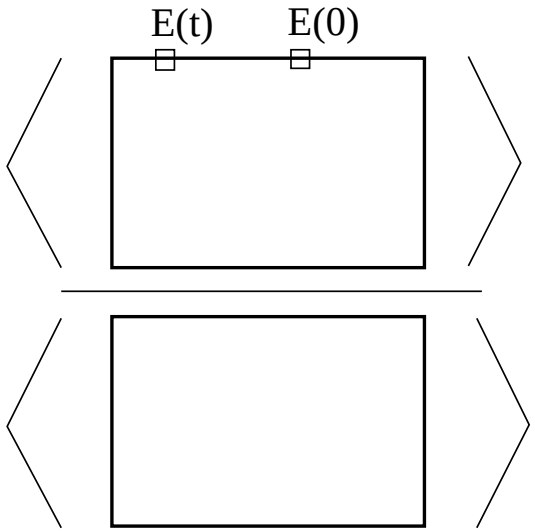

$$V^{(0)}(\mathbf{r}) = \lim_{T\to\infty} \frac{i}{T} \log \langle W_\square \rangle = -C_f \frac{\alpha_s}{r} + \mathcal{O}(\alpha_s^2)$$

$$V^{(1,0)} = -\frac{1}{2} \lim_{T\to\infty} \int_0^T dt\, t\, \langle\!\langle g\mathbf{E}_1(t) \cdot g\mathbf{E}_1(0) \rangle\!\rangle_c = -C_F C_A \frac{\alpha_s^2}{4\, r^2} + \mathcal{O}(\alpha_s^3).$$

$$V^{(2,0)}_{\mathbf{p}^2}(r) = \frac{i}{2} \hat{\mathbf{r}}^i \hat{\mathbf{r}}^j \lim_{T\to\infty} \int_0^T dt\, t^2 \langle\!\langle g\mathbf{E}_1^i(t) g\mathbf{E}_1^j(0) \rangle\!\rangle_c,$$

$$V^{(2,0)}_{\mathbf{L}^2}(r) = \frac{i}{4} \left(\delta^{ij} - 3\hat{\mathbf{r}}^i \hat{\mathbf{r}}^j\right) \lim_{T\to\infty} \int_0^T dt\, t^2 \langle\!\langle g\mathbf{E}_1^i(t) g\mathbf{E}_1^j(0) \rangle\!\rangle_c,$$

$$\begin{aligned}
V_r^{(2,0)}(r) = & -\frac{c_D^{(1)}}{8} \lim_{T\to\infty} \int_0^T dt\, \langle\!\langle [\mathbf{D}_1, g\mathbf{E}_1(t)] \rangle\!\rangle_c \\
& -\frac{i c_F^{(1)\,2}}{4} \lim_{T\to\infty} \int_0^T dt\, \langle\!\langle g\mathbf{B}_1(t) \cdot g\mathbf{B}_1(0) \rangle\!\rangle_c \\
& -\frac{i}{2} \lim_{T\to\infty} \int_0^T dt_1 \int_0^{t_1} dt_2 \int_0^{t_2} dt_3\, (t_2 - t_3)^2 \\
& \qquad \times \langle\!\langle g\mathbf{E}_1(t_1) \cdot g\mathbf{E}_1(t_2) g\mathbf{E}_1(t_3) \cdot g\mathbf{E}_1(0) \rangle\!\rangle_c \\
& +\frac{1}{2} \Big(\boldsymbol{\nabla}_r^i \lim_{T\to\infty} \int_0^T dt_1 \int_0^{t_1} dt_2\, (t_1 - t_2)^2 \\
& \qquad \times \langle\!\langle g\mathbf{E}_1^i(t_1) g\mathbf{E}_1(t_2) \cdot g\mathbf{E}_1(0) \rangle\!\rangle_c \Big) \\
& -\frac{i}{2} \left(\boldsymbol{\nabla}_r^i V^{(0)} \right) \lim_{T\to\infty} \int_0^T dt_1 \int_0^{t_1} dt_2\, (t_1 - t_2)^3
\end{aligned}$$

$$
\begin{aligned}
&\times \langle\!\langle g\mathbf{E}_1^i(t_1) g\mathbf{E}_1(t_2)\cdot g\mathbf{E}_1(0)\rangle\!\rangle_c \\
&-\frac{1}{2}\lim_{T\to\infty}\int_0^T dt_1\int_0^{t_1} dt_2\,(t_1-t_2)^2 \\
&\qquad \times \langle\!\langle [\mathbf{D}_1., g\mathbf{E}_1](t_1) g\mathbf{E}_1(t_2)\cdot g\mathbf{E}_1(0)\rangle\!\rangle_c \\
&+\frac{i}{8}\lim_{T\to\infty}\int_0^T dt\, t^2 \langle\!\langle [\mathbf{D}_1., g\mathbf{E}_1](t)[\mathbf{D}_1., g\mathbf{E}_1](0)\rangle\!\rangle_c \\
&-\frac{i}{4}\big(\boldsymbol{\nabla}_r^i \lim_{T\to\infty}\int_0^T dt\, t^2 \langle\!\langle g\mathbf{E}_1^i(t)[\mathbf{D}_1., g\mathbf{E}_1](0)\rangle\!\rangle_c\big) \\
&-\frac{1}{4}\lim_{T\to\infty}\int_0^T dt\, t^3 \langle\!\langle [\mathbf{D}_1., g\mathbf{E}_1](t) g\mathbf{E}_1^j(0)\rangle\!\rangle_c (\boldsymbol{\nabla}_r^j V^{(0)}) \\
&+\frac{1}{4}\big(\boldsymbol{\nabla}_r^i \lim_{T\to\infty}\int_0^T dt\, t^3 \langle\!\langle g\mathbf{E}_1^i(t) g\mathbf{E}_1^j(0)\rangle\!\rangle_c (\boldsymbol{\nabla}_r^j V^{(0)})\big) \\
&+\frac{1}{2}(\boldsymbol{\nabla}_r^2 V_{\mathbf{p}^2}^{(2,0)}) - \frac{i}{12}\lim_{T\to\infty}\int_0^T dt\, t^4 \\
&\qquad \times \langle\!\langle g\mathbf{E}_1^i(t) g\mathbf{E}_1^j(0)\rangle\!\rangle_c (\boldsymbol{\nabla}_r^i V^{(0)})(\boldsymbol{\nabla}_r^j V^{(0)}) \\
&-d_3'^{(1)} f_{abc}\int d^3\mathbf{x}\lim_{T_W\to\infty} g\langle\!\langle G_{\mu\nu}^a(x) G_{\mu\alpha}^b(x) G_{\nu\alpha}^c(x)\rangle\!\rangle,
\end{aligned}
$$

$$
V_{LS}^{(2,0)}(r) = \frac{c_S^{(1)}}{2r^2}\mathbf{r}\cdot(\boldsymbol{\nabla}_r V^{(0)}) - \frac{c_F^{(1)}}{r^2} i\mathbf{r}\cdot\lim_{T\to\infty}\int_0^T dt\, t\,\langle\!\langle g\mathbf{B}_1(t)\times g\mathbf{E}_1(0)\rangle\!\rangle.
$$

$$
V_{\mathbf{p}^2}^{(1,1)}(r) = i\hat{\mathbf{r}}^i\hat{\mathbf{r}}^j \lim_{T\to\infty}\int_0^T dt\, t^2 \langle\!\langle g\mathbf{E}_1^i(t) g\mathbf{E}_2^j(0)\rangle\!\rangle_c,
$$

$$V^{(1,1)}_{\mathbf{L}^2}(r) = i\frac{\delta^{ij} - 3\hat{\mathbf{r}}^i\hat{\mathbf{r}}^j}{2}\lim_{T\to\infty}\int_0^T dt\, t^2\langle\!\langle g\mathbf{E}_1^i(t) g\mathbf{E}_2^j(0)\rangle\!\rangle_c,$$

$$\begin{aligned}
V^{(1,1)}_r(r) &= -\frac{1}{2}(\boldsymbol{\nabla}_r^2 V^{(1,1)}_{\mathbf{p}^2}) \\
&-i\lim_{T\to\infty}\int_0^T dt_1\int_0^{t_1} dt_2\int_0^{t_2} dt_3\,(t_2-t_3)^2 \\
&\qquad\times\langle\!\langle g\mathbf{E}_1(t_1)\cdot g\mathbf{E}_1(t_2) g\mathbf{E}_2(t_3)\cdot g\mathbf{E}_2(0)\rangle\!\rangle_c \\
&+\frac{1}{2}(\boldsymbol{\nabla}_r^i\lim_{T\to\infty}\int_0^T dt_1\int_0^{t_1} dt_2 (t_1-t_2)^2\langle\!\langle g\mathbf{E}_1^i(t_1) g\mathbf{E}_2(t_2)\cdot g\mathbf{E}_2(0)\rangle\!\rangle_c) \\
&+\frac{1}{2}(\boldsymbol{\nabla}_r^i\lim_{T\to\infty}\int_0^T dt_1\int_0^{t_1} dt_2 (t_1-t_2)^2\langle\!\langle g\mathbf{E}_2^i(t_1) g\mathbf{E}_1(t_2)\cdot g\mathbf{E}_1(0)\rangle\!\rangle_c) \\
&-\frac{i}{2}\left(\boldsymbol{\nabla}_r^i V^{(0)}\right)\lim_{T\to\infty}\int_0^T dt_1\int_0^{t_1} dt_2 (t_1-t_2)^3 \\
&\qquad\times\langle\!\langle g\mathbf{E}_1^i(t_1) g\mathbf{E}_2(t_2)\cdot g\mathbf{E}_2(0)\rangle\!\rangle_c \\
&-\frac{i}{2}\left(\boldsymbol{\nabla}_r^i V^{(0)}\right)\lim_{T\to\infty}\int_0^T dt_1\int_0^{t_1} dt_2 (t_1-t_2)^3 \\
&\qquad\times\langle\!\langle g\mathbf{E}_2^i(t_1) g\mathbf{E}_1(t_2)\cdot g\mathbf{E}_1(0)\rangle\!\rangle_c \\
&-\frac{1}{2}\lim_{T\to\infty}\int_0^T dt_1\int_0^{t_1} dt_2 (t_1-t_2)^2\langle\!\langle [\mathbf{D}_1.,g\mathbf{E}_1](t_1) g\mathbf{E}_2(t_2)\cdot g\mathbf{E}_2(0)\rangle\!\rangle_c \\
&+\frac{1}{2}\lim_{T\to\infty}\int_0^T dt_1\int_0^{t_1} dt_2 (t_1-t_2)^2\langle\!\langle [\mathbf{D}_2.,g\mathbf{E}_2](t_1) g\mathbf{E}_1(t_2)\cdot g\mathbf{E}_1(0)\rangle\!\rangle_c \\
&-\frac{i}{4}\lim_{T\to\infty}\int_0^T dt\, t^2\langle\!\langle [\mathbf{D}_1.,g\mathbf{E}_1](t)[\mathbf{D}_2.,g\mathbf{E}_2](0)\rangle\!\rangle_c
\end{aligned}$$

$$
\begin{aligned}
&+\frac{i}{4}(\boldsymbol{\nabla}_r^i \lim_{T\to\infty}\int_0^T dt\, t^2\{\langle\!\langle g\mathbf{E}_1^i(t)[\mathbf{D}_2.,g\mathbf{E}_2](0)\rangle\!\rangle_c \\
&\qquad -\langle\!\langle g\mathbf{E}_2^i(t)[\mathbf{D}_1.,g\mathbf{E}_1](0)\rangle\!\rangle_c\}) \\
&-\frac{1}{4}\lim_{T\to\infty}\int_0^T dt\, t^3\{\langle\!\langle [\mathbf{D}_1.,g\mathbf{E}_1](t)g\mathbf{E}_2^j(0)\rangle\!\rangle_c \\
&\qquad -\langle\!\langle [\mathbf{D}_2.,g\mathbf{E}_2](t)g\mathbf{E}_1^j(0)\rangle\!\rangle_c\}(\boldsymbol{\nabla}_r^j V^{(0)}) \\
&+\frac{1}{4}(\boldsymbol{\nabla}_r^i \lim_{T\to\infty}\int_0^T dt\, t^3\{\langle\!\langle g\mathbf{E}_1^i(t)g\mathbf{E}_2^j(0)\rangle\!\rangle_c \\
&\qquad +\langle\!\langle g\mathbf{E}_2^i(t)g\mathbf{E}_1^j(0)\rangle\!\rangle_c\}(\boldsymbol{\nabla}_r^j V^{(0)})) \\
&-\frac{i}{6}\lim_{T\to\infty}\int_0^T dt\, t^4\langle\!\langle g\mathbf{E}_1^i(t)g\mathbf{E}_2^j(0)\rangle\!\rangle_c(\boldsymbol{\nabla}_r^i V^{(0)})(\boldsymbol{\nabla}_r^j V^{(0)}) \\
&+(d_{ss}+d_{vs}\lim_{T_W\to\infty}\langle\!\langle T_1^a T_2^a\rangle\!\rangle)\,\delta^{(3)}(\mathbf{x}_1-\mathbf{x}_2),
\end{aligned}
$$

$$
V_{L_2S_1}^{(1,1)}(r) = -\frac{c_F^{(1)}}{r^2} i\mathbf{r}\cdot\lim_{T\to\infty}\int_0^T dt\, t\,\langle\!\langle g\mathbf{B}_1(t)\times g\mathbf{E}_2(0)\rangle\!\rangle,
$$

$$
V_{S^2}^{(1,1)}(r) = \frac{2c_F^{(1)}c_F^{(2)}}{3} i\lim_{T\to\infty}\int_0^T dt\,\langle\!\langle g\mathbf{B}_1(t)\cdot g\mathbf{B}_2(0)\rangle\!\rangle - 4(d_{sv}+d_{vv}\lim_{T_W\to\infty}\langle\!\langle T_1^a T_2^a\rangle\!\rangle)\,\delta^{(3)}(\mathbf{x}_1-\mathbf{x}_2),
$$

$$
V_{\mathbf{S}_{12}}^{(1,1)}(r) = \frac{c_F^{(1)}c_F^{(2)}}{4} i\hat{\mathbf{r}}^i\hat{\mathbf{r}}^j\lim_{T\to\infty}\int_0^T dt\,[\langle\!\langle g\mathbf{B}_1^i(t)\, g\mathbf{B}_2^j(0)\rangle\!\rangle - \frac{\delta^{ij}}{3}\langle\!\langle g\mathbf{B}_1(t)\cdot g\mathbf{B}_2(0)\rangle\!\rangle].
$$

Hamiltonian Formalism

Static limit: $H_{NRQCD} \simeq H^{(0)}$

$$|\underline{\mathrm{n}}; \mathbf{x}_1, \mathbf{x}_2\rangle^{(0)} \equiv \psi^\dagger(\mathbf{x}_1)\chi_c^\dagger(\mathbf{x}_2)|n; \mathbf{x}_1, \mathbf{x}_2\rangle^{(0)}, \qquad E_n^{(0)}(r)$$

$$\left.\begin{array}{l} |\Sigma_g^+; \mathbf{r}\rangle^{(0)} \\ |\Pi; \mathbf{r}\rangle^{(0)} \\ |\Delta; \mathbf{r}\rangle^{(0)} \\ \ldots \end{array}\right\} \text{Spectrum in the static limit}$$

Σ_g^+. Ground state of NRQCD in the static limit.

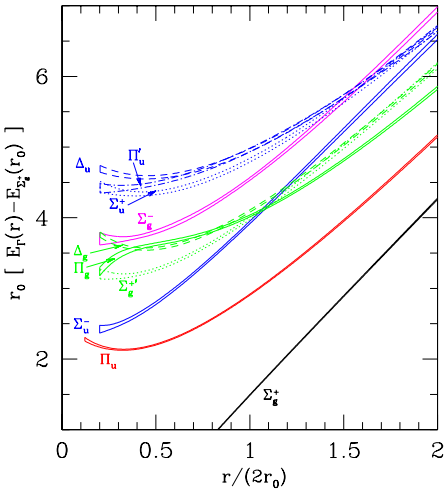

Figure 3: *Energies for different gluonic excitation between static quarks at distance r from the quenched lattice measurements of Juge et al. hep-lat/9809015, $r_0 \simeq 0.5$ fm. The picture is taken from Michael, hep-ph/9809211.*

$$H_{NRQCD} = H^{(0)} + \frac{1}{m} H^{(1)} + \frac{1}{m^2} H^{(2)} + O(1/m^3)$$

$$|\underline{\mathrm{n}}; \mathbf{x}_1, \mathbf{x}_2\rangle, \qquad E_n(\mathbf{x}_1, \mathbf{x}_2, \mathbf{p}_1, \mathbf{p}_2)$$

Matching condition:

$$\boxed{S|0\rangle \equiv |\underline{0}\rangle, \quad E_0(\mathbf{x}_1, \mathbf{x}_2, \mathbf{p}_1, \mathbf{p}_2) = h_s(\mathbf{x}_1, \mathbf{x}_2, \mathbf{p}_1, \mathbf{p}_2)}$$

$O(1/m^0)$

$$\boxed{V_s^{(0)}(r) = E_{\Sigma_g^+}(r)}$$

$O(1/m)$

$$\left[\frac{\mathbf{p}^2}{2} + V^{(1)}(r)\right] \delta^{(3)}(\mathbf{x}_1 - \mathbf{y}_1)\delta^{(3)}(\mathbf{x}_2 - \mathbf{y}_2) = {}^{(0)}\langle \underline{0}; \mathbf{x}_1, \mathbf{x}_2 | H^{(1)} | \underline{0}; \mathbf{y}_1, \mathbf{y}_2 \rangle^{(0)}$$

$$= \left(-\frac{{\boldsymbol{\nabla}_{\mathbf{x}_1}}^2}{2} + \frac{1}{2} \sum_{n \neq 0} \left| \frac{{}^{(0)}\langle n | g\mathbf{E} | 0 \rangle^{(0)}}{E_0^{(0)} - E_n^{(0)}} \right|^2 \right) \delta^{(3)}(\mathbf{x}_1 - \mathbf{y}_1)\delta^{(3)}(\mathbf{x}_2 - \mathbf{y}_2).$$

We have used

a) ${}^{(0)}\langle n | \mathbf{D}_{\mathbf{x}_1} | n \rangle^{(0)} = \boldsymbol{\nabla}_{\mathbf{x}_1}$, b) ${}^{(0)}\langle n | \mathbf{D}_{\mathbf{x}_1} | j \rangle^{(0)} = \dfrac{{}^{(0)}\langle n | g\mathbf{E}(\mathbf{x}_1) | j \rangle^{(0)}}{E_n^{(0)} - E_j^{(0)}} \quad \forall\, n \neq j,$

Finally

$$V^{(1)}(r) = \frac{1}{2} \sum_{n \neq 0} \left| \frac{{}^{(0)}\langle n | g\mathbf{E} | 0 \rangle^{(0)}}{E_0^{(0)} - E_n^{(0)}} \right|^2 .$$

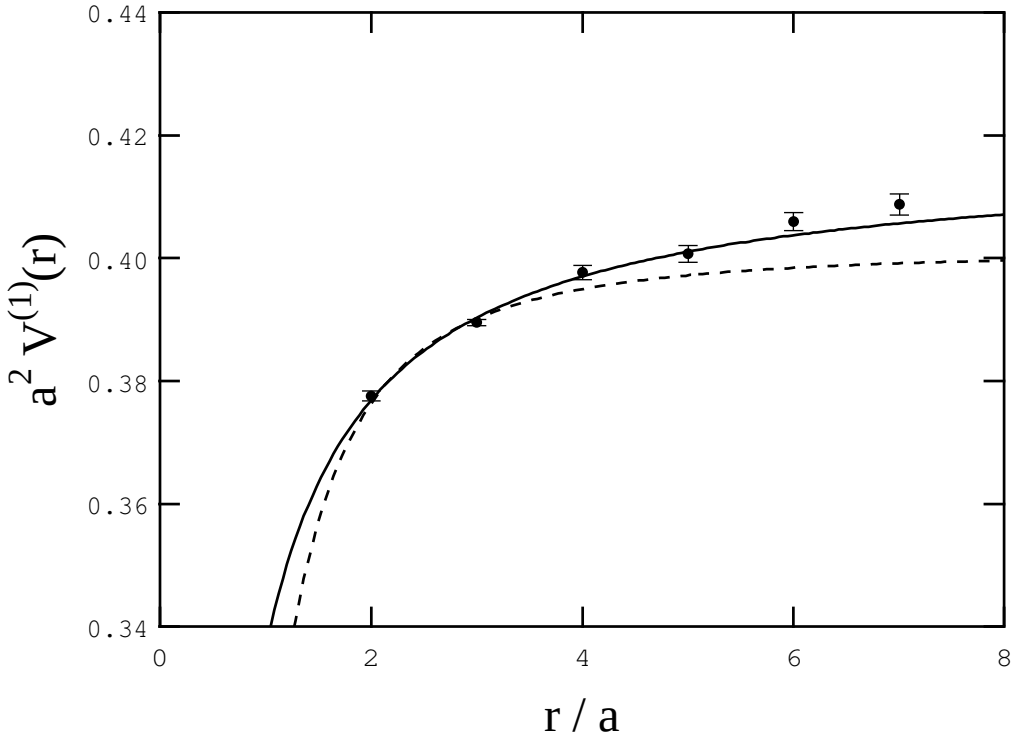

Figure 4: $V^{(1)}$ *from Koma, Koma and Wittig, hep-lat/0607009.*

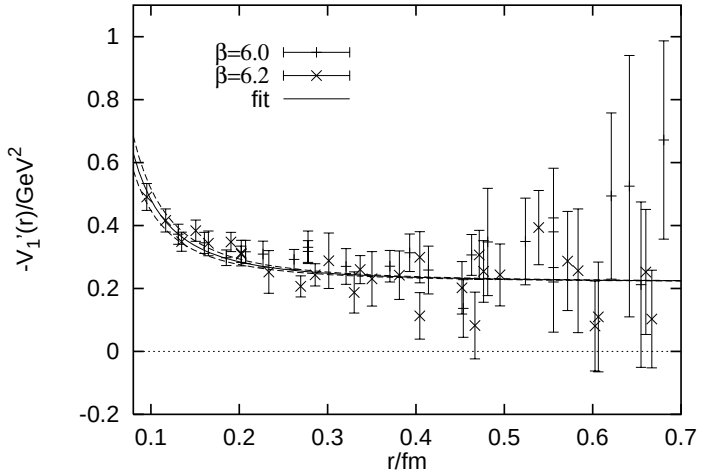

Figure 5: *The spin-orbit potential $-V_1'$ with the fit $\sigma + h/r^2$ from Bali, Schilling and Wachter, 1997. The lattice simulations are quenched. The fitting parameters are $\sigma \approx (468\ MeV)^2$ and $h \approx 0.067$.*

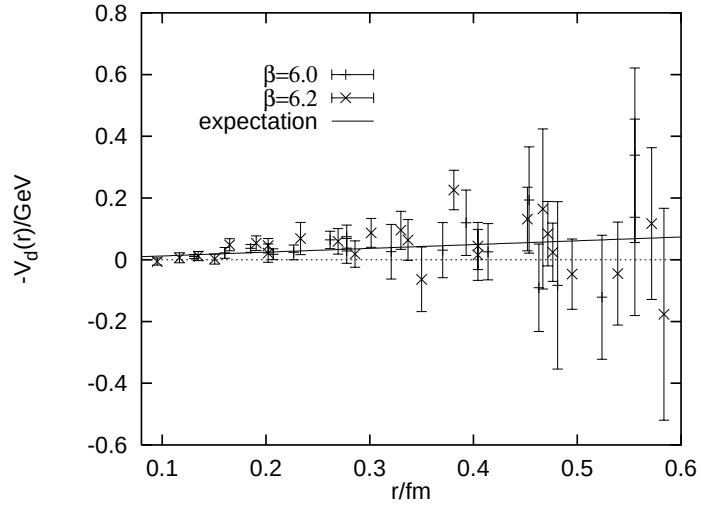

Figure 6: *The potential V_d together with the curve $-\sigma/9\,r$, from Bali, Schilling and Wachter, 1997. The lattice simulations are quenched. The fitting parameters are $\sigma \approx (468\ MeV)^2$ and $h \approx 0.067$.*

Symmetries of the static limit of NRQCD

The gluonic excitations between heavy quarks have the symmetries of a diatomic molecule (plus charge conjugation)

Energy eigenstates are clasified in terms of:

a) $|L_z| = 0, 1, 2, ... = \Sigma, \Pi, \Delta, ...$;

b) CP (u/g);

c) Reflection $(+/-)$ (only for Σ states).

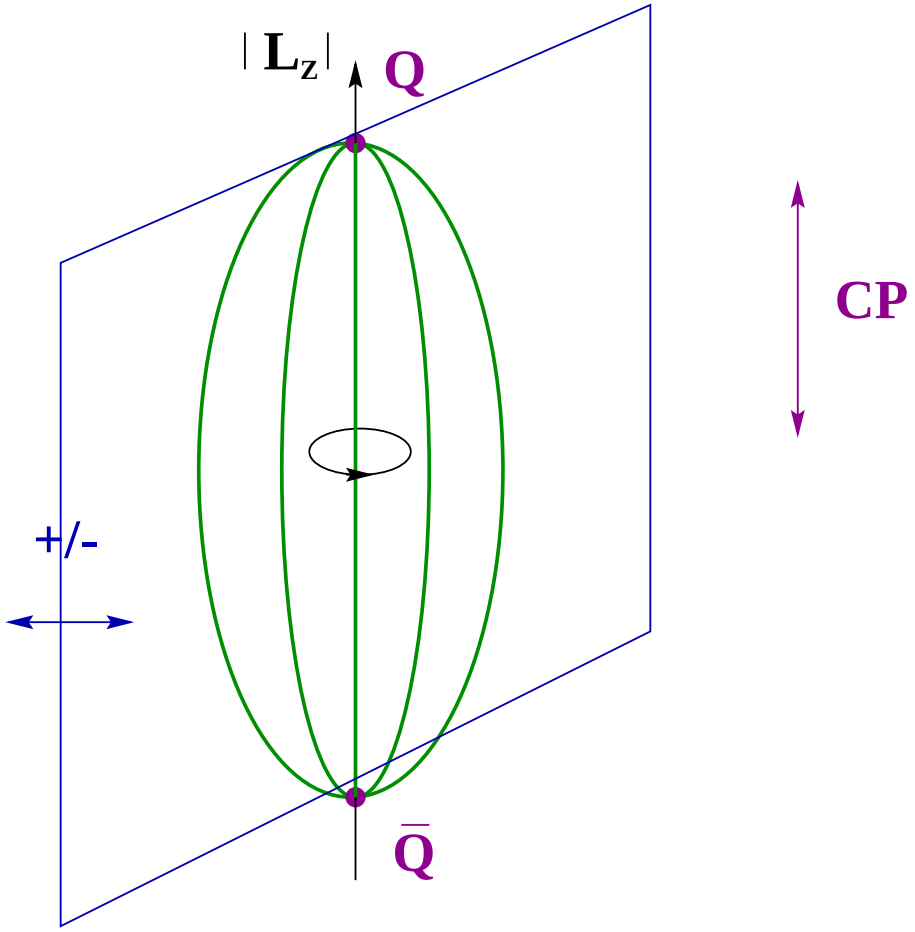

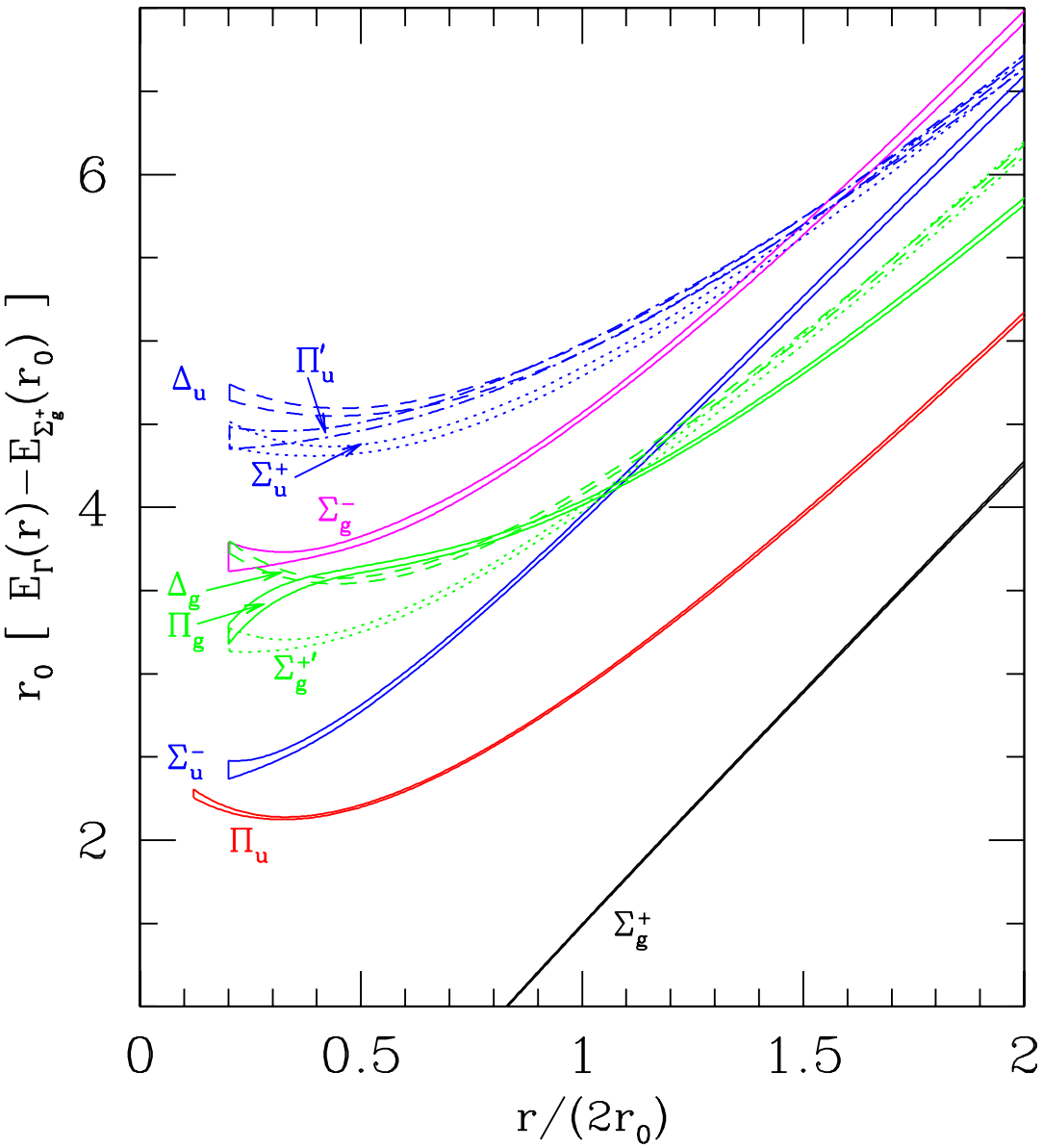

Figure 7: *Energies for different gluonic excitation between static quarks. Juge et al. hep-lat/9809015,* $r_0 \simeq 0.5$ *fm.*

pNRQCD: the static limit $O(1/m^0)$

$$\mathcal{L}_{pNRQCD} = \mathrm{Tr}\Big\{S^\dagger \Big(i\partial_0 - V_s^{(0)}(\mathbf{x})\Big) S + O^\dagger \Big(iD_0 - V_o^{(0)}(\mathbf{x})\Big) O\Big\} + \mathcal{O}(r),$$

Extra (approximate) symmetries in the effective theory.

NRQCD: $D_{\infty h}$ (substituting parity by CP).

pNRQCD: $O(3)\times$C. Softly broken by the multipole expansion.

Degeneracies:

$$\Sigma_g^{+\prime} \sim \Pi_g \,; \qquad \Sigma_g^- \sim \Pi_g' \sim \Delta_g \,; \qquad \Sigma_u^- \sim \Pi_u \,; \qquad \Sigma_u^+ \sim \Pi_u' \sim \Delta_u \,.$$

Gluelumps $O^a H^a$	$L=1$	$L=2$
$\Sigma_g^{+\prime}$	$\mathbf{r}\cdot\mathbf{E}\,, \mathbf{r}\cdot(\mathbf{D}\times\mathbf{B})$	
Σ_g^-		$(\mathbf{r}\cdot\mathbf{D})(\mathbf{r}\cdot\mathbf{B})$
Π_g	$\mathbf{r}\times\mathbf{E}\,, \mathbf{r}\times(\mathbf{D}\times\mathbf{B})$	
Π_g'		$\mathbf{r}\times((\mathbf{r}\cdot\mathbf{D})\mathbf{B}+\mathbf{D}(\mathbf{r}\cdot\mathbf{B}))$
Δ_g		$(\mathbf{r}\times\mathbf{D})^i(\mathbf{r}\times\mathbf{B})^j+(\mathbf{r}\times\mathbf{D})^j(\mathbf{r}\times\mathbf{B})^i$
Σ_u^+		$(\mathbf{r}\cdot\mathbf{D})(\mathbf{r}\cdot\mathbf{E})$
Σ_u^-	$\mathbf{r}\cdot\mathbf{B}\,, \mathbf{r}\cdot(\mathbf{D}\times\mathbf{E})$	
Π_u	$\mathbf{r}\times\mathbf{B}\,, \mathbf{r}\times(\mathbf{D}\times\mathbf{E})$	
Π_u'		$\mathbf{r}\times((\mathbf{r}\cdot\mathbf{D})\mathbf{E}+\mathbf{D}(\mathbf{r}\cdot\mathbf{E}))$
Δ_u		$(\mathbf{r}\times\mathbf{D})^i(\mathbf{r}\times\mathbf{E})^j+(\mathbf{r}\times\mathbf{D})^j(\mathbf{r}\times\mathbf{E})^i$

Table 1: *Operators H for the Σ, Π and Δ gluonic excitations between static quarks in pNRQCD up to dimensions 3. The covariant derivative is understood in the adjoint representation. $\mathbf{D}\cdot\mathbf{B}$ and $\mathbf{D}\cdot\mathbf{E}$ do not appear, the first because it is identically zero after using the Jacobi identity, while the second gives vanishing contributions after using the equations of motion. Brambilla-Pineda-Vairo-Soto(1999).*

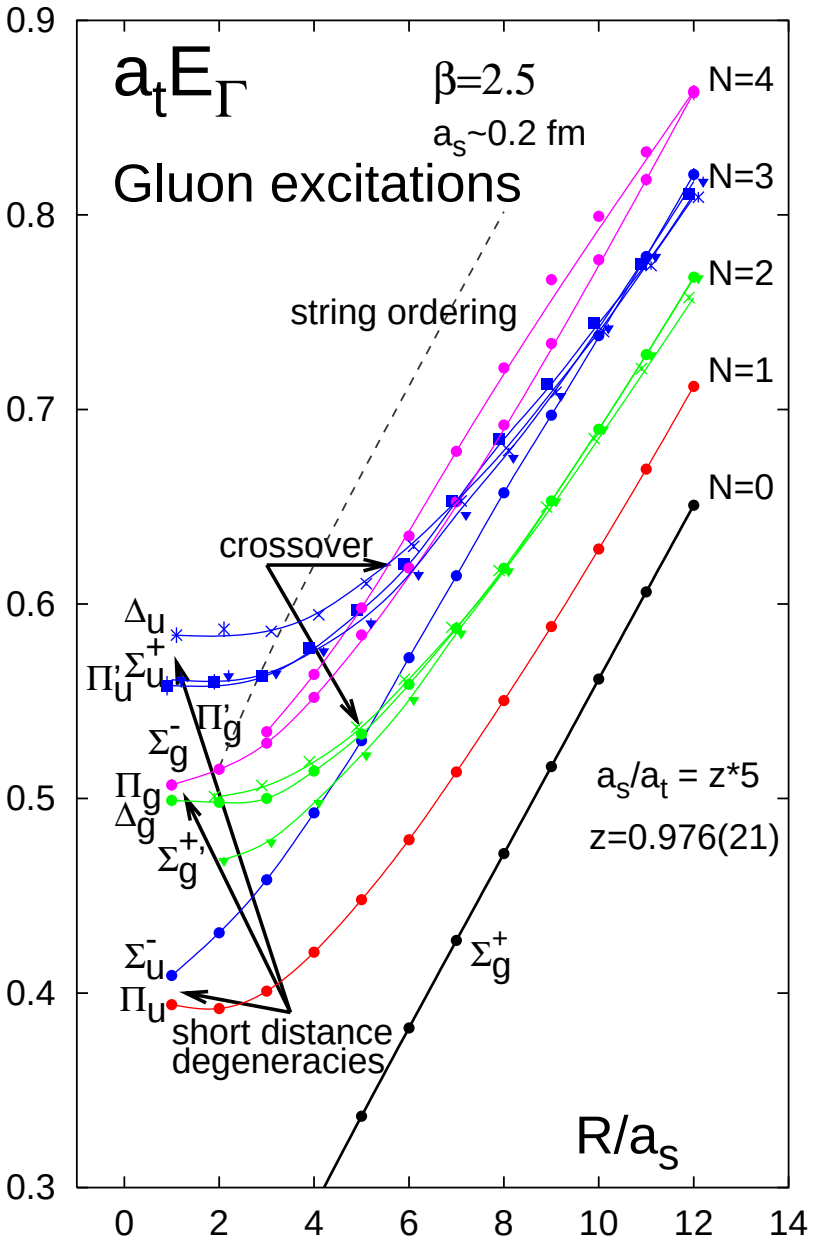

Figure 8: *Energies for different gluonic excitation between static quarks. Juge et al. hep-lat/0207004.*

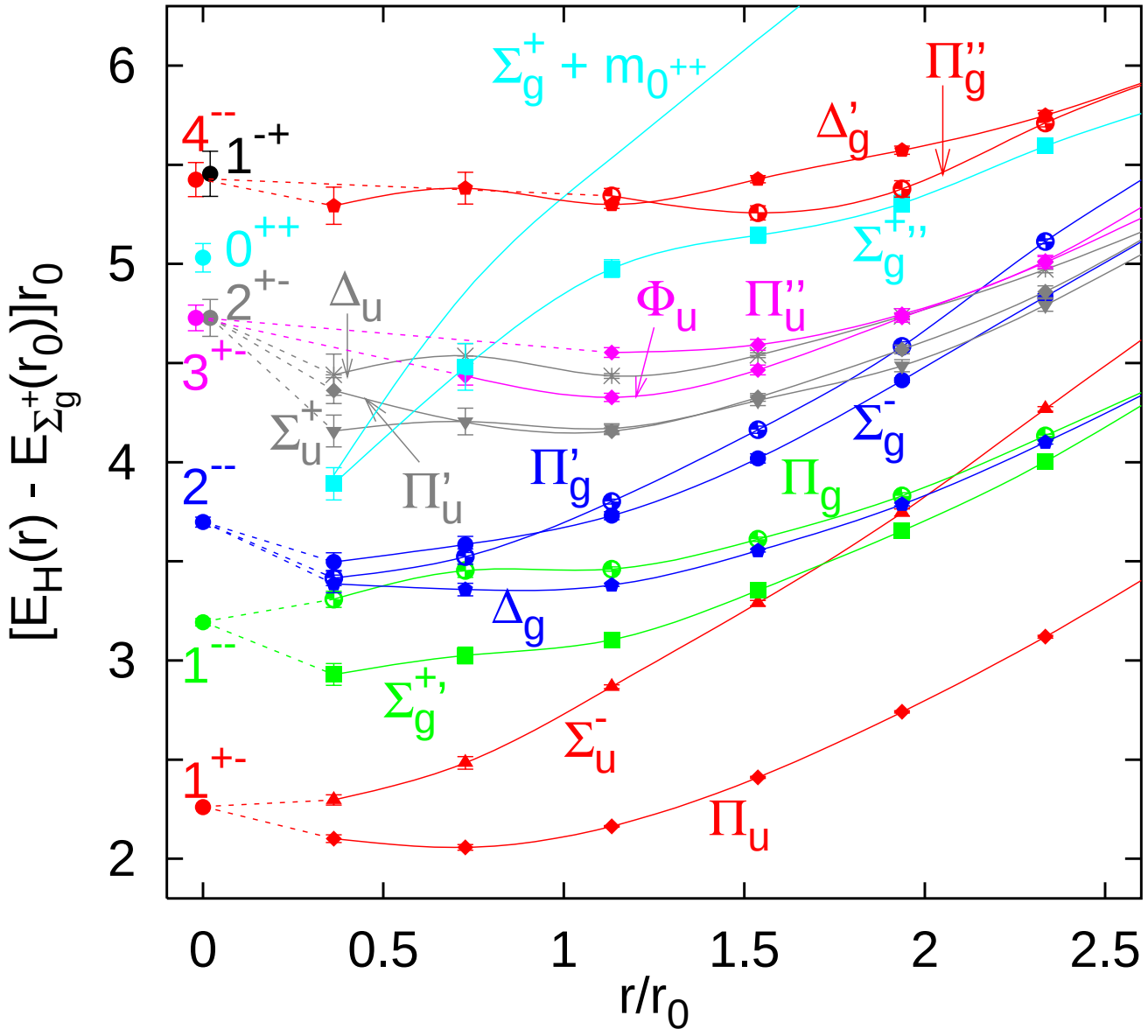

Figure 9: Different hybrid potentials Juge et al. 2003 at a lattice spacing $a_\sigma \approx 0.2$ fm $\approx 0.4\, r_0$, where $r_0 \approx 0.5$ fm, in comparison with the gluelump spectrum, extrapolated to the continuum limit Foster and Michael, 1999 (circles, left-most data points). The gluelump spectrum has been shifted by an arbitrary constant to adjust the 1^{+-} state with the Π_u and Σ_u^- potentials at short distance. In addition, we include the sum of the ground state (Σ_g^+) potential and the scalar glueball mass $m_{0^{++}}$ Bali et al., 1993; Lucini and Teper, 2001; Morningstar and Peardon, 1999. The lines are drawn to guide the eye. Bali-Pineda 2004

point particle J^{PC}	open string $\Lambda_\eta^{\sigma_v}$
1^{+-}	Σ_u^-, Π_u
1^{--}	$\Sigma_g^{+\prime}, \Pi_g$
2^{--}	$\Sigma_g^-, \Pi_g', \Delta_g$
2^{+-}	$\Sigma_u^+, \Pi_u', \Delta_u$
3^{+-}	$\Sigma_u^{-'}, \Pi_u'', \Delta_u', \Phi_u$
0^{++}	$\Sigma_g^{+\prime\prime}$
4^{--}	$\Sigma_g^{-\prime}, \Pi_g'', \Delta_g', \Phi_g, \Gamma_g$
1^{-+}	$\Sigma_u^{+\prime}, \Pi_u'''$

Table 2: Expected degeneracies of hybrid potentials at short distance, based on the level ordering of the gluelump spectrum. Note that if the 3^{+-} gluelump turned out to be lighter than the 2^{+-} then the $\Sigma_u^{-'}, \Pi_u', \Delta_u, \Phi_u$ potentials would approach the 3^{+-} state while the $\Sigma_u^+, \Pi_u'', \Delta_u'$ potentials would approach the 2^{+-} instead. Bali-Pineda04

J^{PC}	H	$(\Lambda_H - \Lambda_B)r_0$	$(\Lambda_H - \Lambda_B)$/GeV
1^{--}	E_i	0.93	0.38
2^{--}	$D_{\{i}B_{j\}}$	1.44	0.58
2^{+-}	$D_{\{i}E_{j\}}$	2.47	0.99
3^{+-}	$D_{\{i}D_jB_{k\}}$	2.47	0.99
0^{++}	$\mathbf{B}^2$	2.77	1.11
4^{--}	$D_{\{i}D_jD_kB_{l\}}$	3.16	1.26
1^{-+}	$(\mathbf{B}\wedge\mathbf{E})_i$	3.20	1.28

Table 3: Differences for the gluelump masses (normalized to the B gluelump mass) in the continuum limit in r_0 units and in GeV. Foster and Michael (1999). Note that we can not fix the continuum limit of Λ_B or, in other words, the absolute normalization of the gluelump masses.

$$V_H(r) = V_o(r) + \Lambda_H + \mathcal{O}(r^2), \qquad V_o(r) = \frac{\alpha_s}{2N_c}\frac{1}{r} + \cdots$$

$$\langle H^a(T/2)\phi(T/2,-T/2)^{\rm adj}_{ab}H^b(-T/2)\rangle^{\rm nonpert.} \simeq h\, e^{-i\Lambda_H T} + h'\, e^{-i\Lambda_H' T} + \ldots .$$

The static singlet potential

The introduction of renormalons allows to obtain agreement between lattice simulations and perturbation theory.

$$E_s = 2m_{\rm OS} + V_{s,\rm OS} + \mathcal{O}(r^2)$$

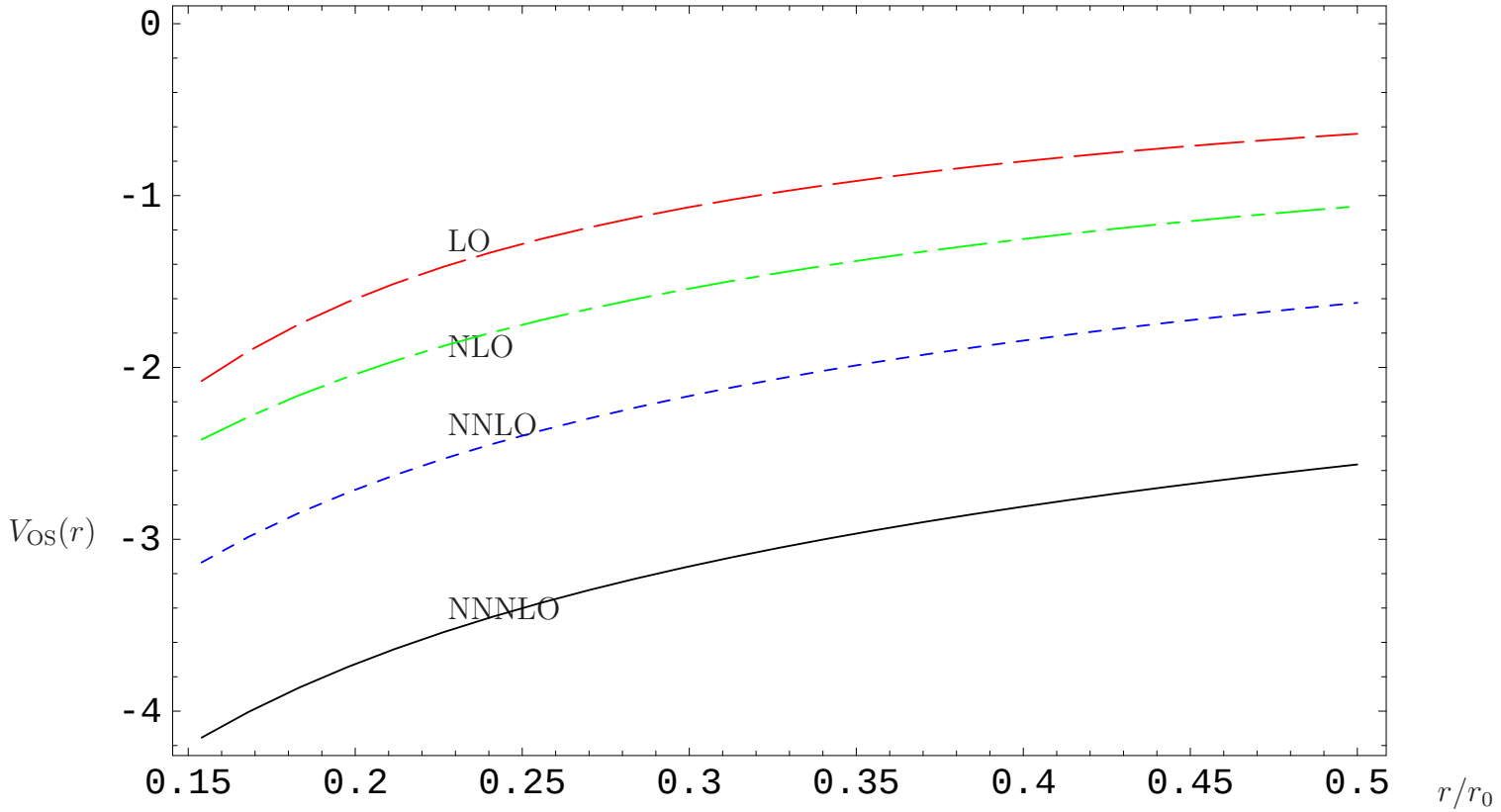

Figure 10: *Plot of* $V_{\rm OS}(r)$ *at tree (dashed line), one-loop (dash-dotted line), two-loops (dotted line) and three loops (estimate) plus the leading single ultrasoft log (solid line). For the scale of* $\alpha_s(\nu)$ $\nu =$ *constant.* $\nu_{us} = 2.5\, r_0^{-1}$.

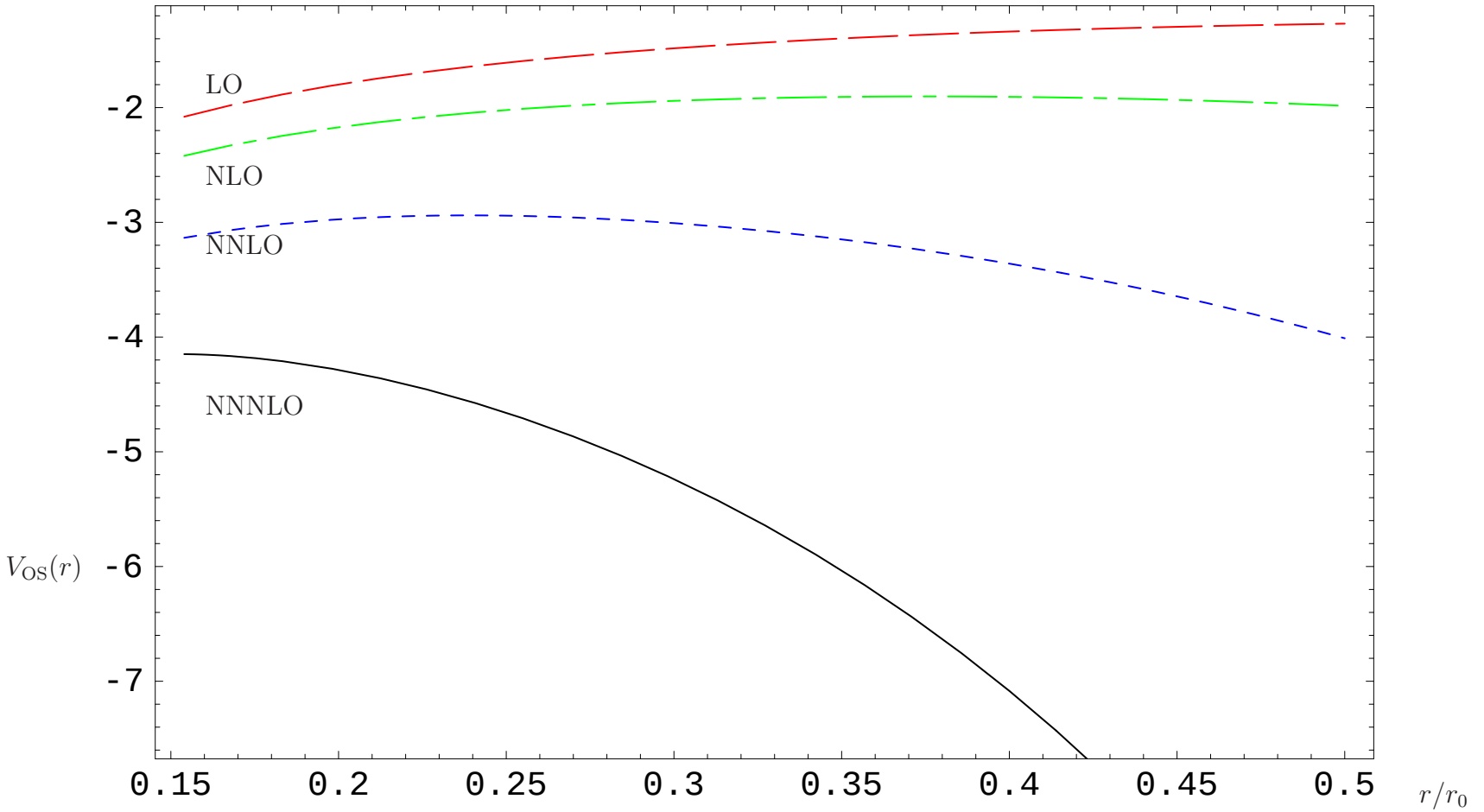

Figure 11: *Plot of* $V_{\rm OS}(r)$ *at tree (dashed line), one-loop (dash-dotted line), two-loops (dotted line) and three loops (estimate) plus the RG expression for the ultrasoft logs (solid line). For the scale of* $\alpha_s(\nu)$*, we set* $\nu = 1/r$*.* $\nu_{us} = 2.5\, r_0^{-1}$*.*

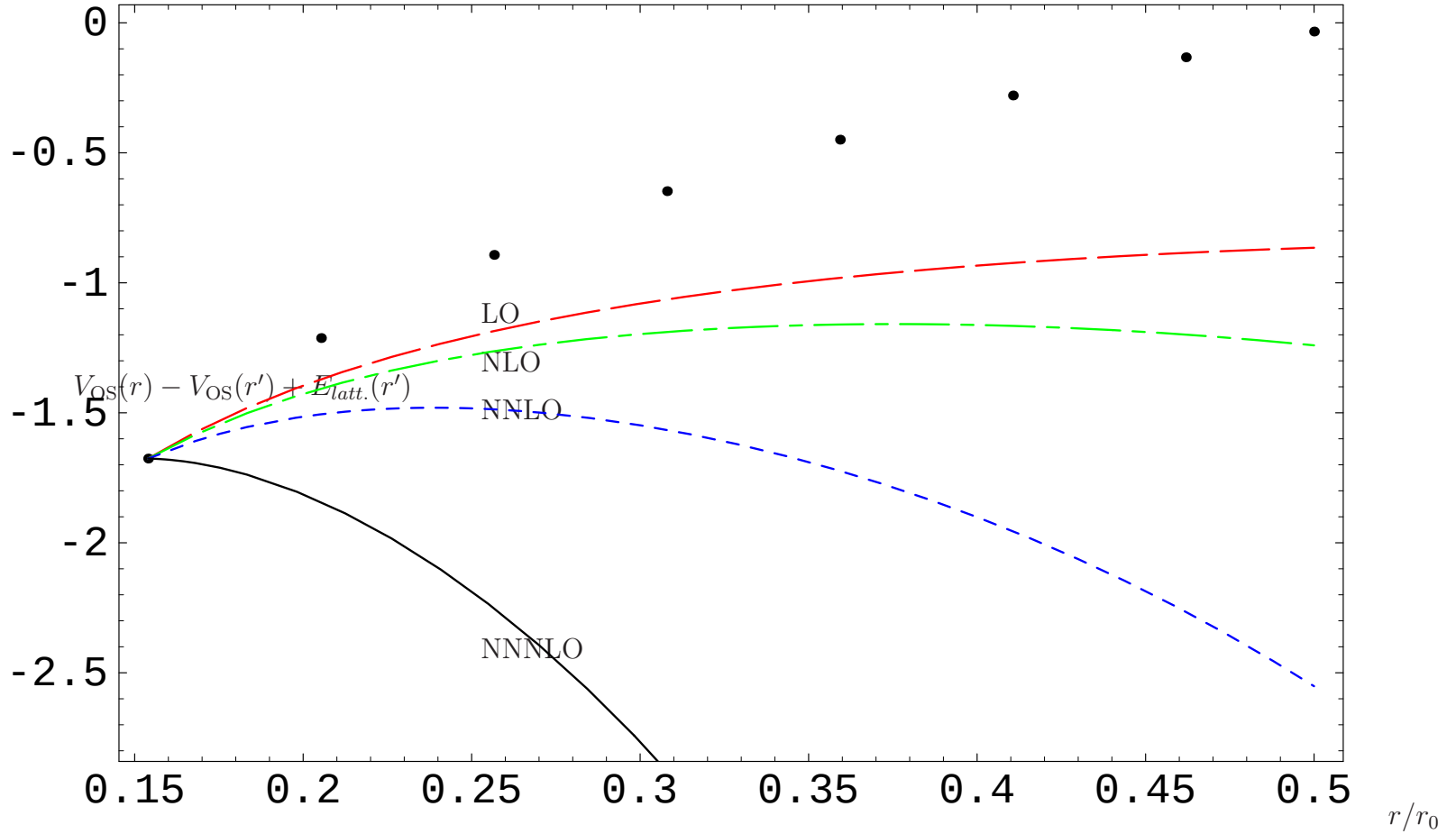

Figure 12: *Plot of* $V_{\rm OS}(r) - V_{\rm OS}(r') + E_{latt.}(r')$ *versus* r *at tree (dashed line), one-loop (dash-dotted line), two-loops (dotted line) and three loops (estimate) plus the RG expression for the ultrasoft logs (solid line) compared with the lattice simulations of Necco and Sommer. For the scale of* $\alpha_s(\nu)$*, we set* $\nu = 1/r$*.* $\nu_{us} = 2.5\, r_0^{-1}$*.*

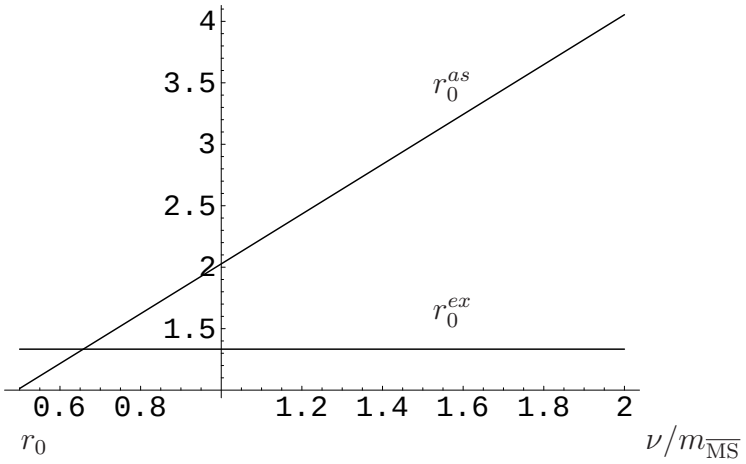

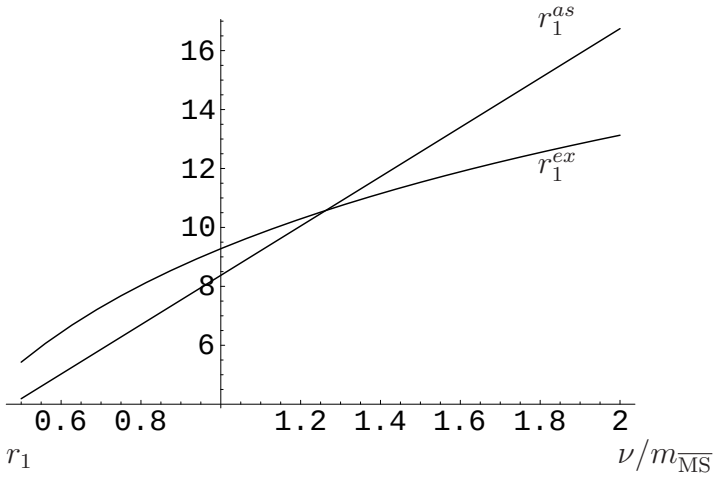

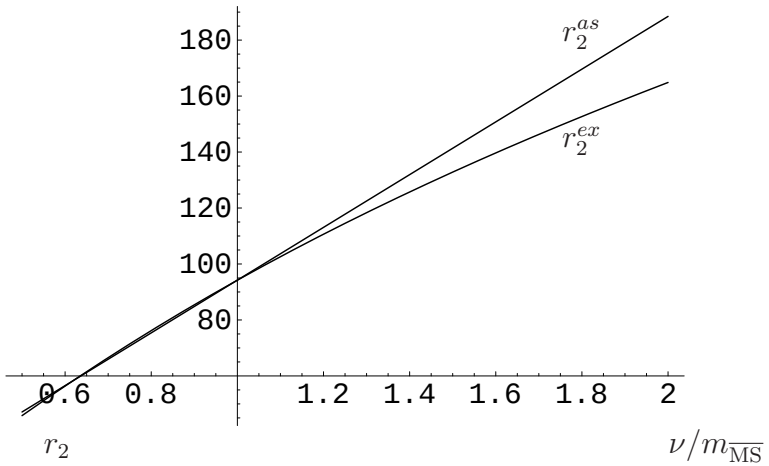

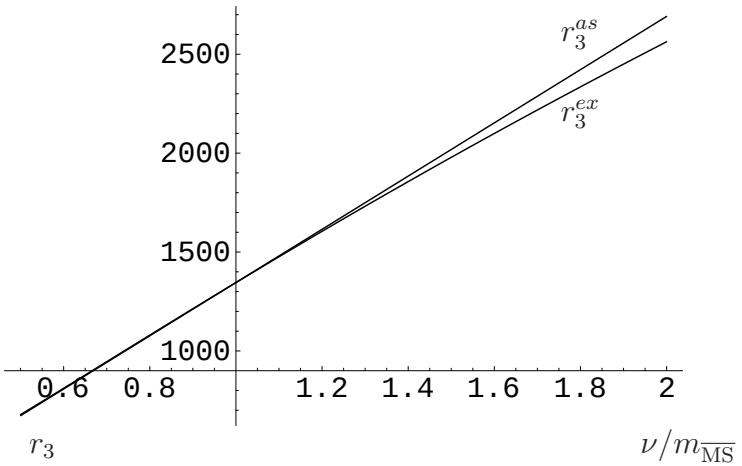

$$m_{\rm OS} = m_{\overline{\rm MS}} + \sum_{n=0}^{\infty} r_n \alpha_s^{n+1} \,,$$

$$r_n^{as} \overset{n\to\infty}{=} N_m \, \nu \left(\frac{\beta_0}{2\pi}\right)^n \frac{\Gamma(n+1+b)}{\Gamma(1+b)} \left(1 + \frac{b}{(n+b)} c_1 + \frac{b(b-1)}{(n+b)(n+b-1)} c_2 + \cdots\right).$$

$$E_s = 2m_{\rm RS}(\nu_f) + V_{s,\rm RS}(\nu_f) + \mathcal{O}(r^2)$$

$$m_{\rm RS}(\nu_f) = m_{\rm OS} - \sum_{n=0}^{\infty} N_m \, \nu_f \left(\frac{\beta_0}{2\pi}\right)^n \alpha_s^{n+1}(\nu_f) \sum_{k=0}^{\infty} c_k \frac{\Gamma(n+1+b-k)}{\Gamma(1+b-k)} \, .$$

Expansion in $\alpha_s(\nu)$

$$m_{\rm RS}(\nu_f) = m_{\overline{\rm MS}} + \sum_{n=0}^{\infty} r_n^{\rm RS} \alpha_s^{n+1} \, ,$$

where $r_n^{\rm RS} = r_n^{\rm RS}(m_{\overline{\rm MS}}, \nu, \nu_f)$. They are the ones expected to be of natural size. We now do not loose accuracy if we first obtain $m_{\rm RS}$ and later on $m_{\overline{\rm MS}}$.

$$V^{(0)}_{s,\rm RS(RS')}(\nu_f) = V_s^{(0)} + 2\delta m_{\rm RS(RS')} \, ,$$

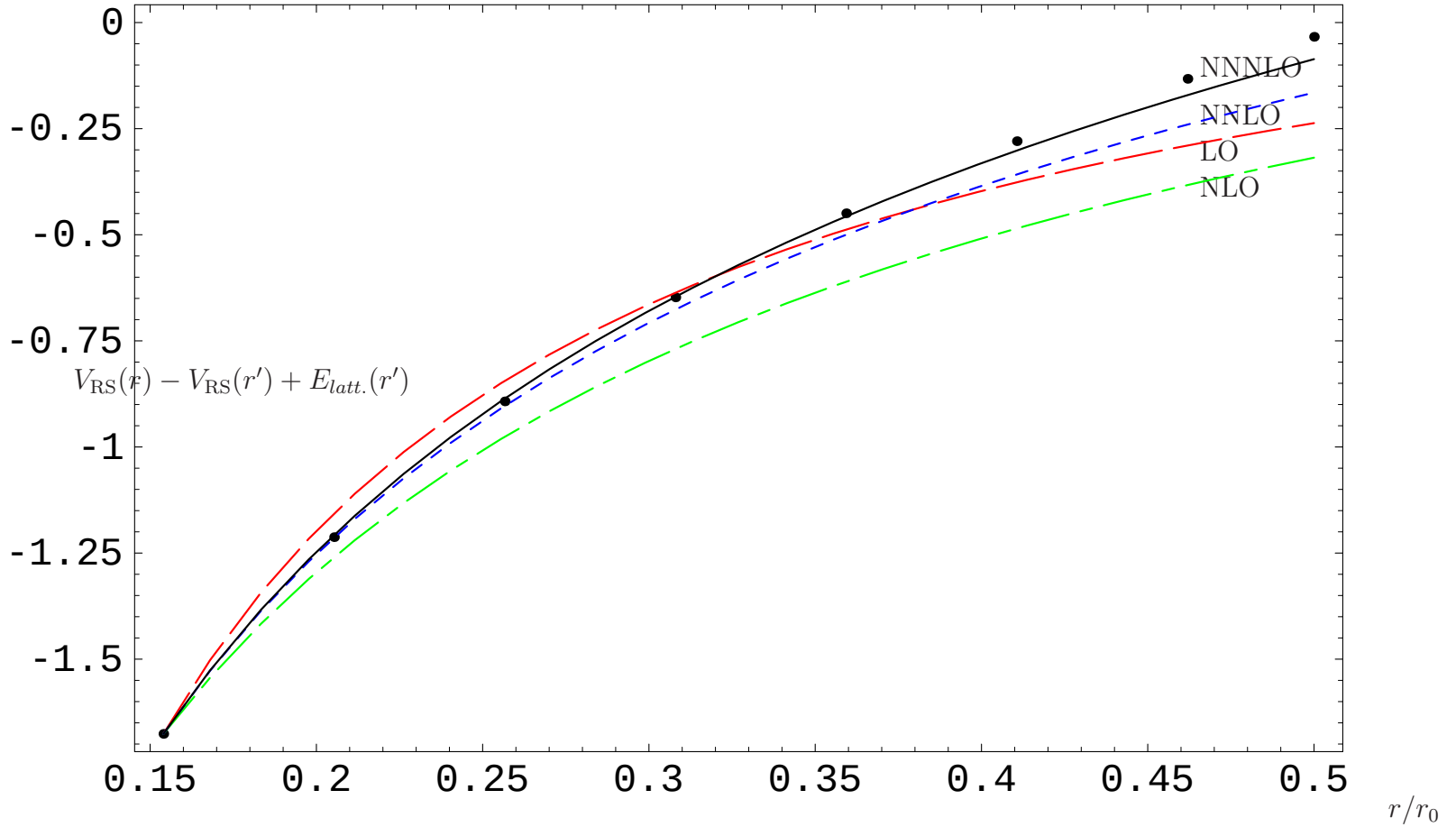

Figure 13: *Plot of* $V_{\rm RS}(r) - V_{\rm RS}(r') + E_{latt.}(r')$ *versus* r *at tree (dashed line), one-loop (dash-dotted line), two-loops (dotted line) and three loops (estimate) plus the leading single ultrasoft log (solid line) compared with the lattice simulations of Necco and Sommer. For the scale of* $\alpha_s(\nu)$ $\nu = constant$. $\nu_{us} = 2.5\, r_0^{-1}$.

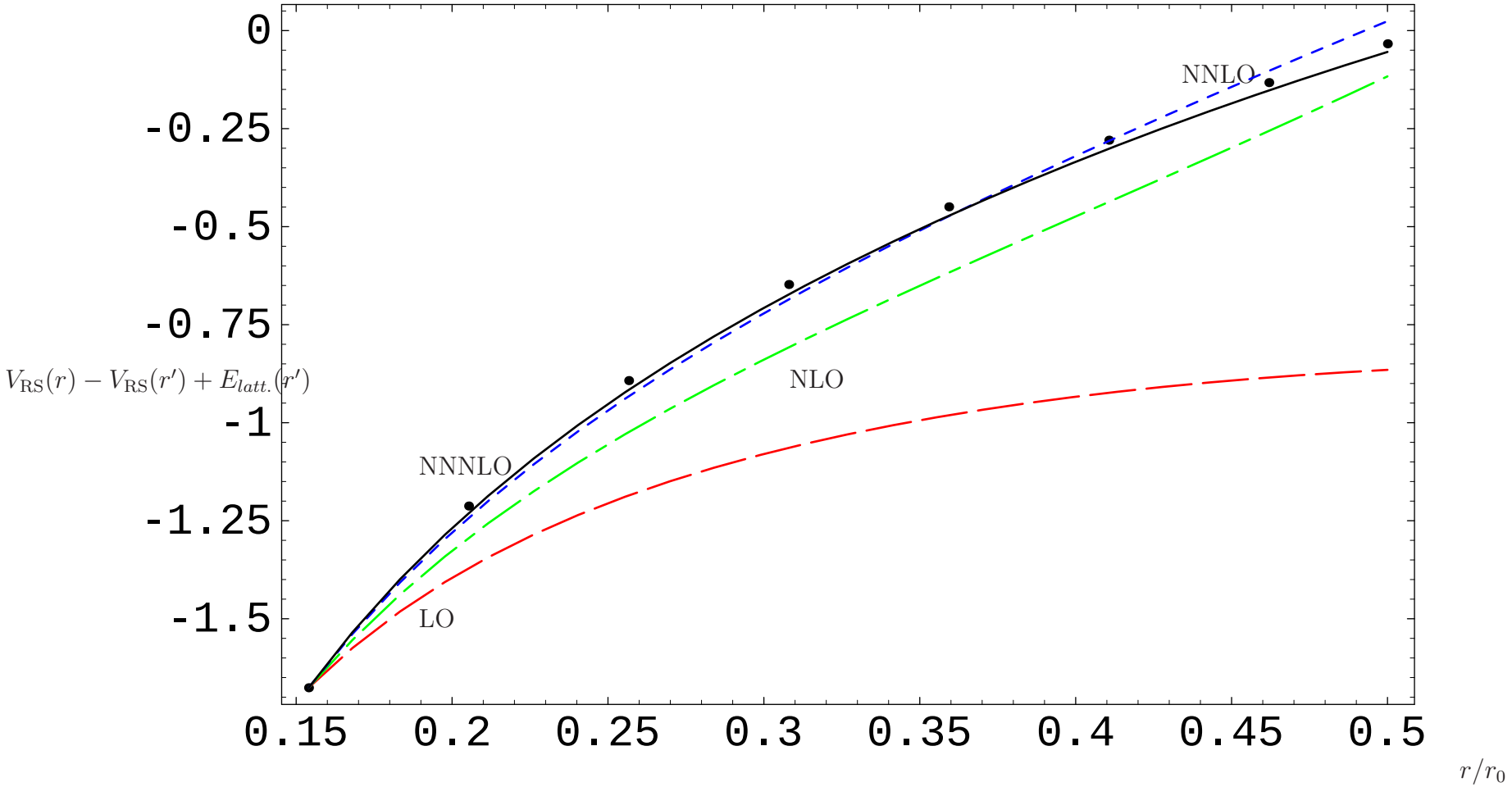

Figure 14: *Plot of* $V_{\rm RS}(r) - V_{\rm RS}(r') + E_{latt.}(r')$ *versus* r *at tree (dashed line), one-loop (dash-dotted line), two-loops (dotted line) and three loops (estimate) plus the RG expression for the ultrasoft logs (solid line) compared with the lattice simulations of Necco and Sommer. For the scale of* $\alpha_s(\nu)$*, we set* $\nu = 1/r$*.* $\nu_f = \nu_{us} = 2.5\, r_0^{-1}$.

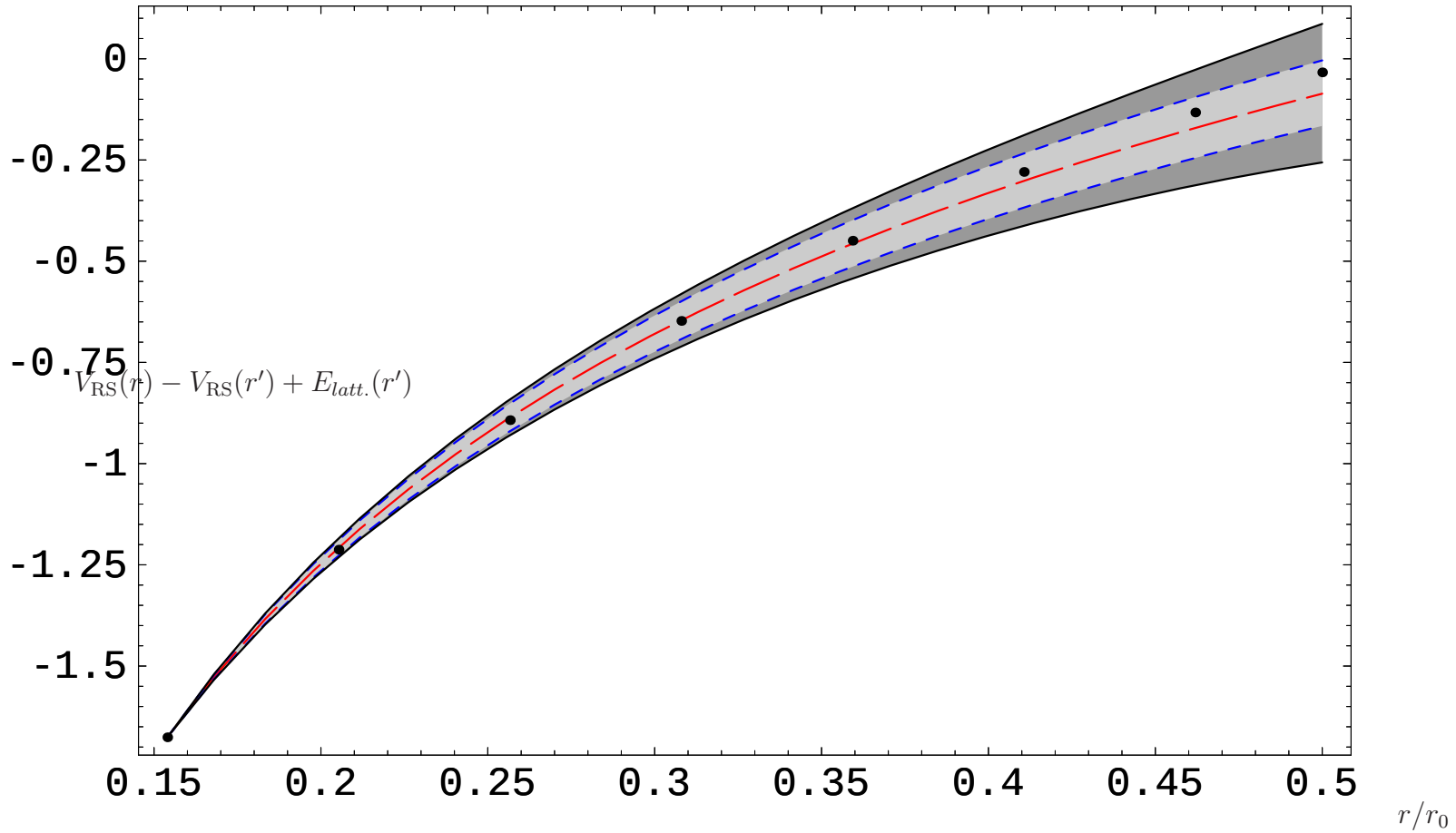

Figure 15: *Plot of* $V_{\rm RS}(r) - V_{\rm RS}(r') + E_{latt.}(r')$ *versus* r *at tree (dashed line), one-loop (dash-dotted line), two-loops (dotted line) and three loops (estimate) plus the leading single ultrasoft log (solid line) compared with the lattice simulations of Necco and Sommer. For the scale of* $\alpha_s(\nu)$ $\nu = constant$. $\nu_{us} = 2.5\, r_0^{-1}$.

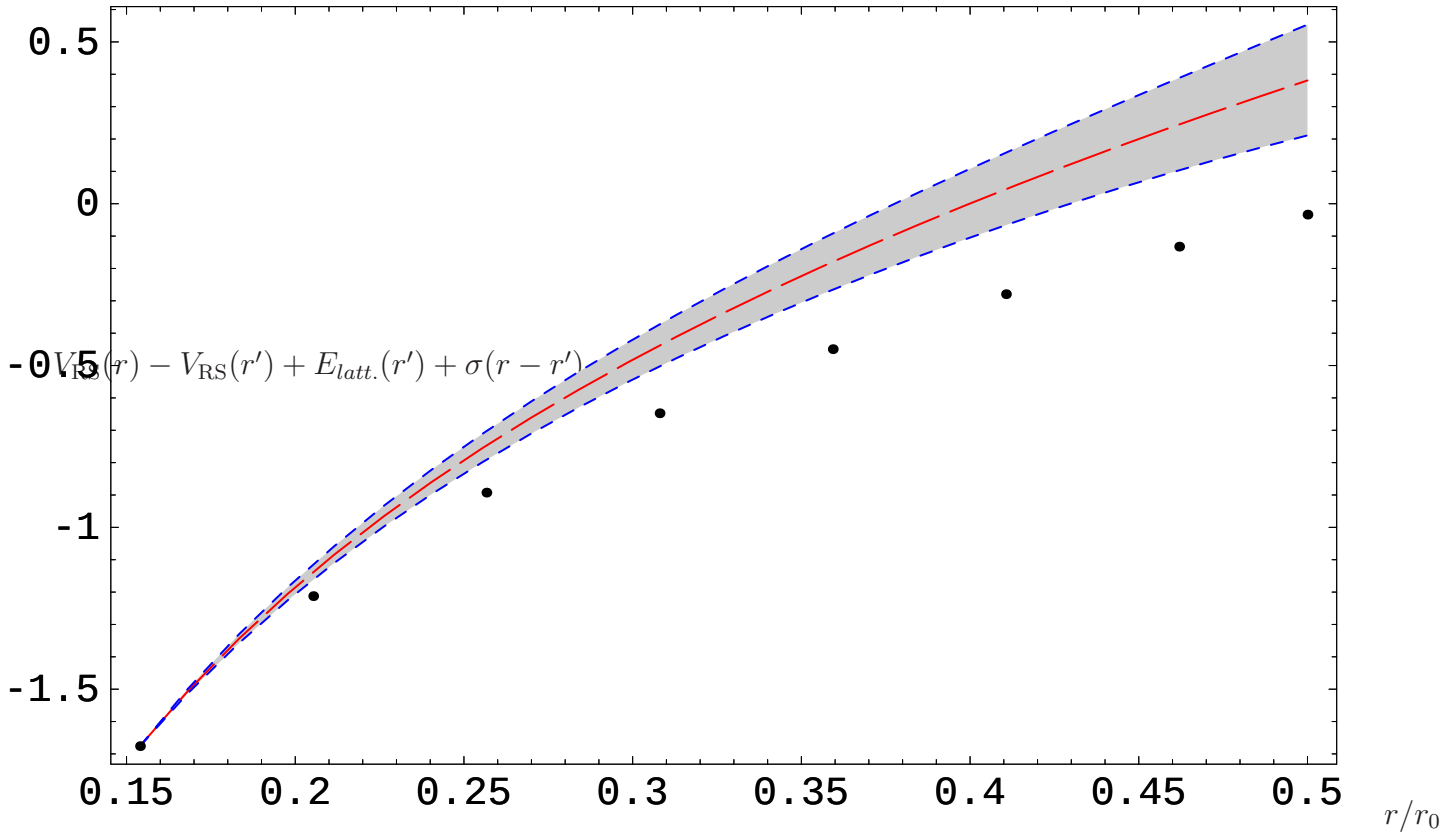

Figure 16: *Plot of* $V_{\rm RS}(r) - V_{\rm RS}(r') + E_{latt.}(r') + \sigma(r - r')$ *versus* r *at three loops (estimate) with the leading ultrasoft log compared with the lattice simulations of Necco and Sommer. For the scale of* $\alpha_s(\nu)$*, we set* $\nu =$ *constant.* $\sigma = 1.35\, r_0^{-2}$ *and* $\nu_{us} = 2.5\, r_0^{-1}$.

1) Perturbation theory works very well for energies above 1 GeV (Pineda; Sumino, Recksiegel; Lee (Necco, Sommer for the force)).

2) Constraint on the size of nonperturbative effecs for heavy quarkonium.

3) A linear non-perturbative potential at short distances is ruled out.

Static Hybrids versus gluelumps

$$E_H = 2m_{\rm OS} + V_{o,{\rm OS}} + \Lambda_H^{\rm OS} + \mathcal{O}(r^2)$$

$$E_H = 2m_{\rm RS}(\nu_f) + V_{o,{\rm RS}}(\nu_f) + \Lambda_H^{\rm RS}(\nu_f) + \mathcal{O}(r^2)$$

$$E_H = 2m_{\rm latt}(1/a) + V_{o,{\rm latt}}(1/a) + \Lambda_H^{\rm latt}(1/a) + \mathcal{O}(r^2)$$

$$V_o = \frac{1}{2N_c}\frac{\alpha_s}{r} + \cdots ({\rm two-loops: Kniehl, Penin, Schroeder, Smirnov, Steinhauser})$$

$$2N_m + N_{V_o} + N_\Lambda = 0$$

Factorization scale $\nu_f \leftrightarrow 1/a$; $\delta m_{\rm RS}(\nu_f)$, $\delta\Lambda_{\rm RS}(\nu_f)$; $\delta m_{\rm latt}(1/a)$, $\delta\Lambda_{\rm latt}(1/a)$.

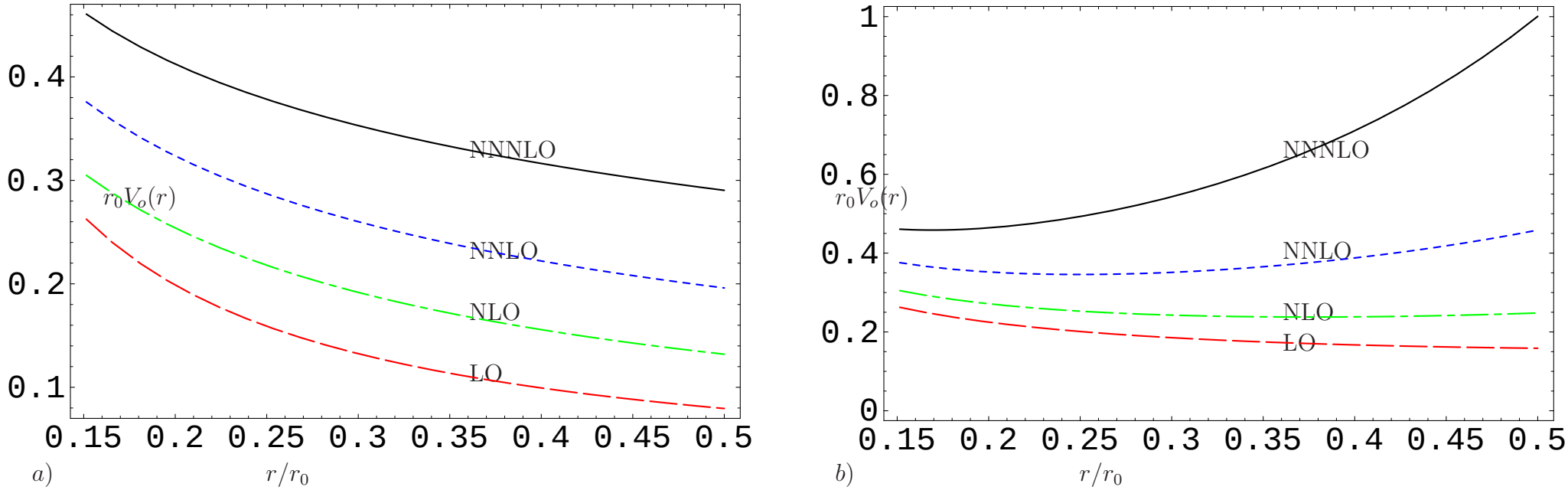

Figure 17: $r_0 V_o(r)$ *(the octet potential in the OS scheme) at tree level (dashed lines), one-loop (dashed-dotted lines), two loops (dotted lines) and three loops (estimate) plus the leading single ultrasoft log (solid lines). Fig. a) corresponds to the scale* $\nu = \nu_i$ *and Fig. b) to* $\nu = 1/r$*. In both cases,* $\nu_{us} = 2.5\, r_0^{-1}$*. Only the solid curves depend on this choice.*

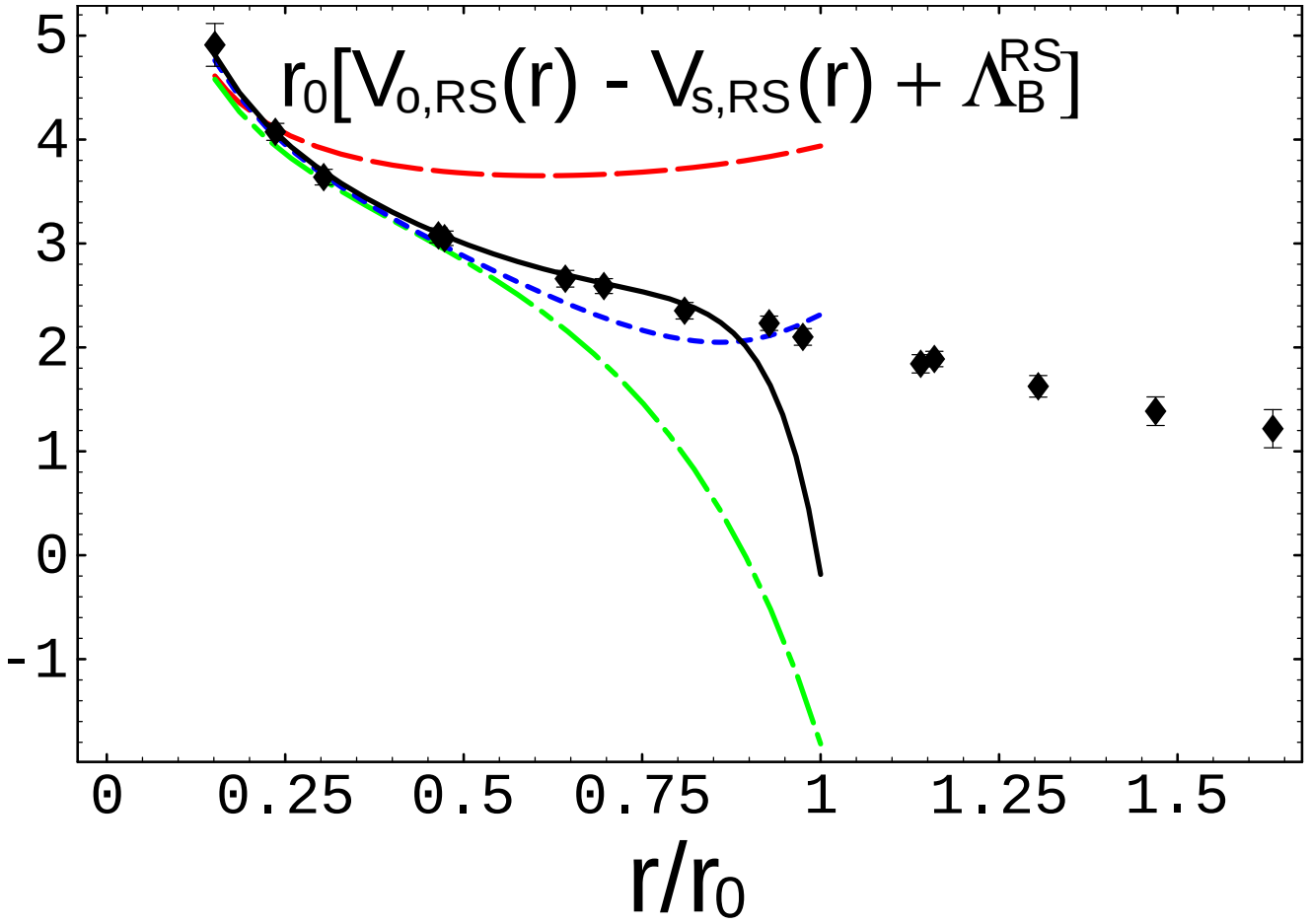

Figure 18: Splitting between the Π_u and the Σ_g^+ potentials and the comparison with the theoretical prediction with $\nu = 1/r$ for $\nu_f = 2.5\, r_0^{-1}$. $r_0[(V_{o,\mathrm{RS}} - V_{s,\mathrm{RS}})(r) + \Lambda_B^{\mathrm{RS}}]$ is plotted versus r at tree level (dashed line), one-loop (dashed-dotted line), two-loops (dotted line) and three loops (estimate) plus the RG expression for the ultrasoft logs (solid line). Bali-Pineda 2004.

Table 4: Absolute values for the gluelump masses in the continuum limit in the RS scheme at $\nu_f = 2.5\, r_0^{-1} \approx 1$ GeV, in r_0 units and in GeV. Note that an additional uncertainty of about 10 % should be added to the last column to account for the quenched approximation. We also display examples of creation operators H for these states. The curly braces denote complete symmetrization of the indices. Bali-Pineda 2004.

J^{PC}	H	$\Lambda_H^{\rm RS} r_0$	$\Lambda_H^{\rm RS}/\mathrm{GeV}$
1^{+-}	B_i	2.25(39)	0.87(15)
1^{--}	E_i	3.18(41)	1.25(16)
2^{--}	$D_{\{i}B_{j\}}$	3.69(42)	1.45(17)
2^{+-}	$D_{\{i}E_{j\}}$	4.72(48)	1.86(19)
3^{+-}	$D_{\{i}D_jB_{k\}}$	4.72(45)	1.86(18)
0^{++}	$\mathbf{B}^2$	5.02(46)	1.98(18)
4^{--}	$D_{\{i}D_jD_kB_{l\}}$	5.41(46)	2.13(18)
1^{-+}	$(\mathbf{B} \wedge \mathbf{E})_i$	5.45(51)	2.15(20)

Heavy-light systems

$$M_B = m_{\rm RS}(\nu_f) + \bar{\Lambda}^{\rm RS}(\nu_f) + \mathcal{O}(1/m)$$

$$M_B = m_{\rm latt}(1/a) + \bar{\Lambda}^{\rm latt}(1/a) + \mathcal{O}(1/m)$$

$$\boxed{\bar{\Lambda}^{\rm RS}(2.5\, r_0^{-1}) = [1.17 \pm 0.08(\text{latt.}) \pm 0.13(\text{th.}) \pm 0.09(\Lambda_{\overline{\rm MS}})]\, r_0^{-1}\,.}$$

$$\boxed{m_{b,\overline{\rm MS}}(m_{b,\overline{\rm MS}}) = [4191 \pm 29(\text{latt.}) \pm 47(\text{th.}) \pm 1(\Lambda_{\overline{\rm MS}})]\ \text{MeV}\,.}$$

Perturbative running of $1/a$

$$2(\bar{\Lambda}_L(1/a) - \bar{\Lambda}_L(1/a')) = V_{s,L}(r;1/a) - V_{s,L}(r;1/a') = C_F\left(\frac{1}{a} - \frac{1}{a'}\right) v_1\alpha_s + \cdots .$$

$$\begin{aligned}\Lambda_H^L(1/a) - \Lambda_H^L(1/a') &= [V_{o,L}(r;1/a) - V_{s,L}(r;1/a)] - [V_{o,L}(r;1/a') - V_{s,L}(r;1/a')] \\ &= \frac{C_A}{2}\left(\frac{1}{a} - \frac{1}{a'}\right) v_1'\alpha_s + \cdots ,\end{aligned}$$

$$\bar{\Lambda}_{\rm pot}^L(a) = \frac{1}{2}V_s^L(r_0;a) + \Delta.$$

$$\left.\begin{array}{ccc} \bar{\Lambda}_L(1/a) & \Longleftrightarrow & \bar{\Lambda}_L(1/a') \\ \Updownarrow\ (\nu_f = 1/a) & & \Updownarrow\ (\nu_f' = 1/a') \\ \bar{\Lambda}_{\rm RS}(\nu_f) & \Longleftrightarrow & \bar{\Lambda}_{\rm RS}(\nu_f') \end{array}\right\} \text{The circle can be closed using perturbation theory}$$

and a similar circle applies for $V_s^L(r;1/a)$, $V_o^L(r;1/a)$ and $\Lambda_H^L(1/a)$.

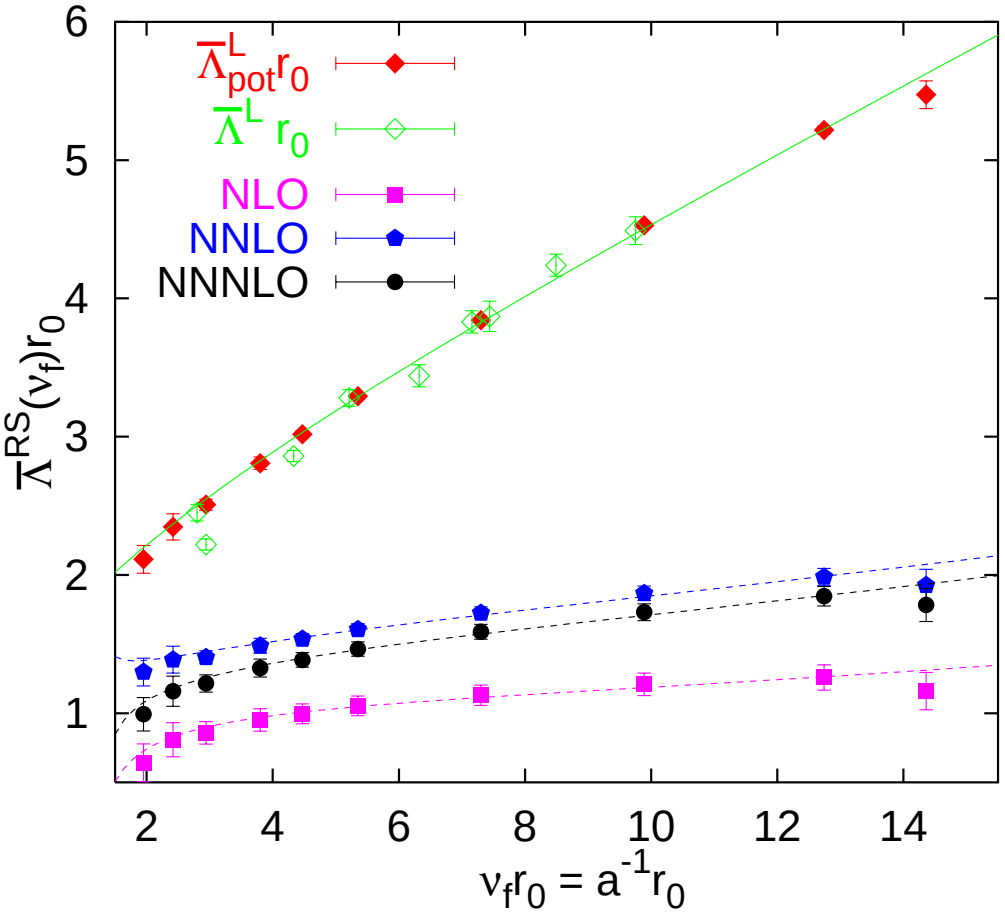

Figure 19: The binding energy $\overline{\Lambda}^{L}_{\rm pot}$, in the lattice scheme (full diamonds), in comparison with $\overline{\Lambda}^{L}$ (open diamonds). The constant Δ has been adjusted by requiring agreement between the two data sets at $r_0 \approx 7.3\, a$. The uncertainty of $\Delta = (0.988 \pm 0.067)\, r_0^{-1}$ is not included into the errors. NLO, NNLO and NNNLO refer to transformations of $\overline{\Lambda}^{L}_{\rm pot}$ into the RS scheme to different orders in perturbation theory. The solid line corresponds to the NNNLO expectation with $\Lambda_{\overline{\rm MS}} \approx 0.602\, r_0^{-1}$, and the central value, $\overline{\Lambda}^{\rm RS}(\nu_f = 9.76\, r_0^{-1}) = 1.70\, r_0^{-1}$. Bali-Pineda 2004.

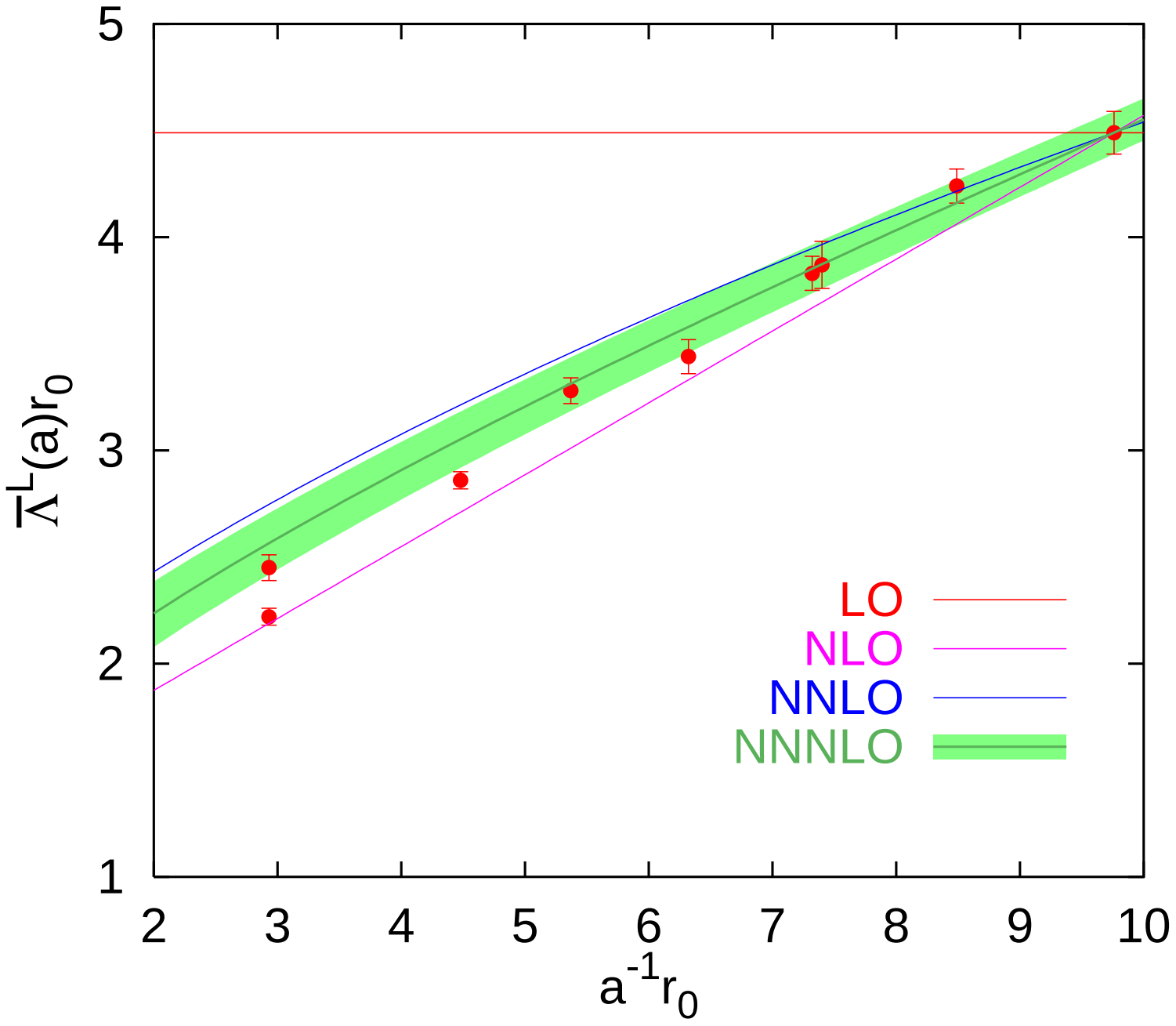

Figure 20: Perturbative running of the binding energy $\overline{\Lambda}$ in the lattice scheme, in comparison with lattice data, starting at the smallest available lattice spacing. The NNNLO error band incorporates the error due to the uncertainty in $\Lambda_{\overline{\rm MS}}$, and the statistical error. Bali-Pineda(2004).

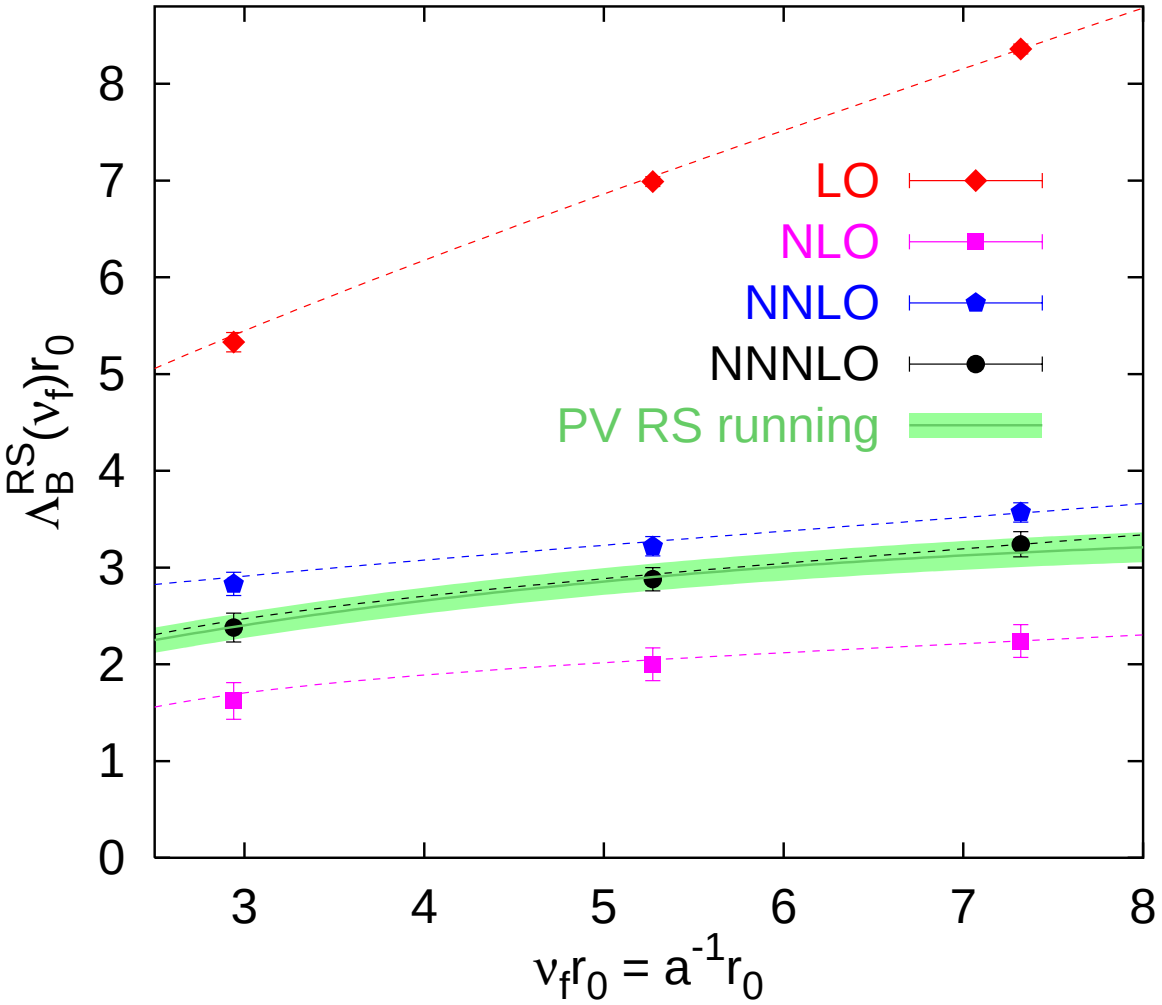

Figure 21: *The lowest gluelump mass Λ_B^L as obtained on the lattice (diamonds), as well as converted into the RS scheme at NLO (squares), NNLO (pentagons) and NNNLO* (NNNLO estimate, circles). The error band corresponds to the result for $\Lambda_B^{\rm RS}$ without the "theoretical" error, run to different scales, according to the PV prescription. Bali-Pineda 2004.*

Conclusions

- Potentials appear in the description of heavy quarkonium from first principles using effective field theories.
- (static, relativistic and hybrid) Potentials can be obtained from the spectrum of static NRQCD.
- The short distance behavior of the hybrid potentials is related with the physics of the gluelumps.
- Very good description of the (lattice) static singlet and octet potential at short distances is obtained with perturbation theory once a renormalon free working scheme is used.
- The absolute value (normalization) of potentials and gluelump masses can only be obtained after taking into account renormalon effects.
- Running of $1/a$ can be predicted by perturbation theory. No need for small lattice spacing simulations.
- Determination of the gluelump masses, $\bar{\Lambda}$ and m_b mass from lattice. Very good agreement with the direct determinations from phenomenology.

$$\Lambda_B^{\rm RS}(2.5\,r_0^{-1}) = [2.25 \pm 0.10(\text{latt.}) \pm 0.21(\text{th.}) \pm 0.08(\Lambda_{\overline{\rm MS}})]\, r_0^{-1}\,,$$

$$\Lambda_B^{\rm RS}(1\,\text{GeV}) = [887 \pm 39(\text{latt.}) \pm 83(\text{th.}) \pm 32(\Lambda_{\overline{\rm MS}})]\,\text{MeV}\,.$$

$$\overline{\Lambda}^{\rm RS}(2.5\,r_0^{-1}) = [1.17 \pm 0.08(\text{latt.}) \pm 0.13(\text{th.}) \pm 0.09(\Lambda_{\overline{\rm MS}})]\, r_0^{-1}\,,$$

$$m_{b,\overline{\rm MS}}(m_{b,\overline{\rm MS}}) = [4191 \pm 29(\text{latt.}) \pm 47(\text{th.}) \pm 1(\Lambda_{\overline{\rm MS}})]\,\text{MeV}\,.$$

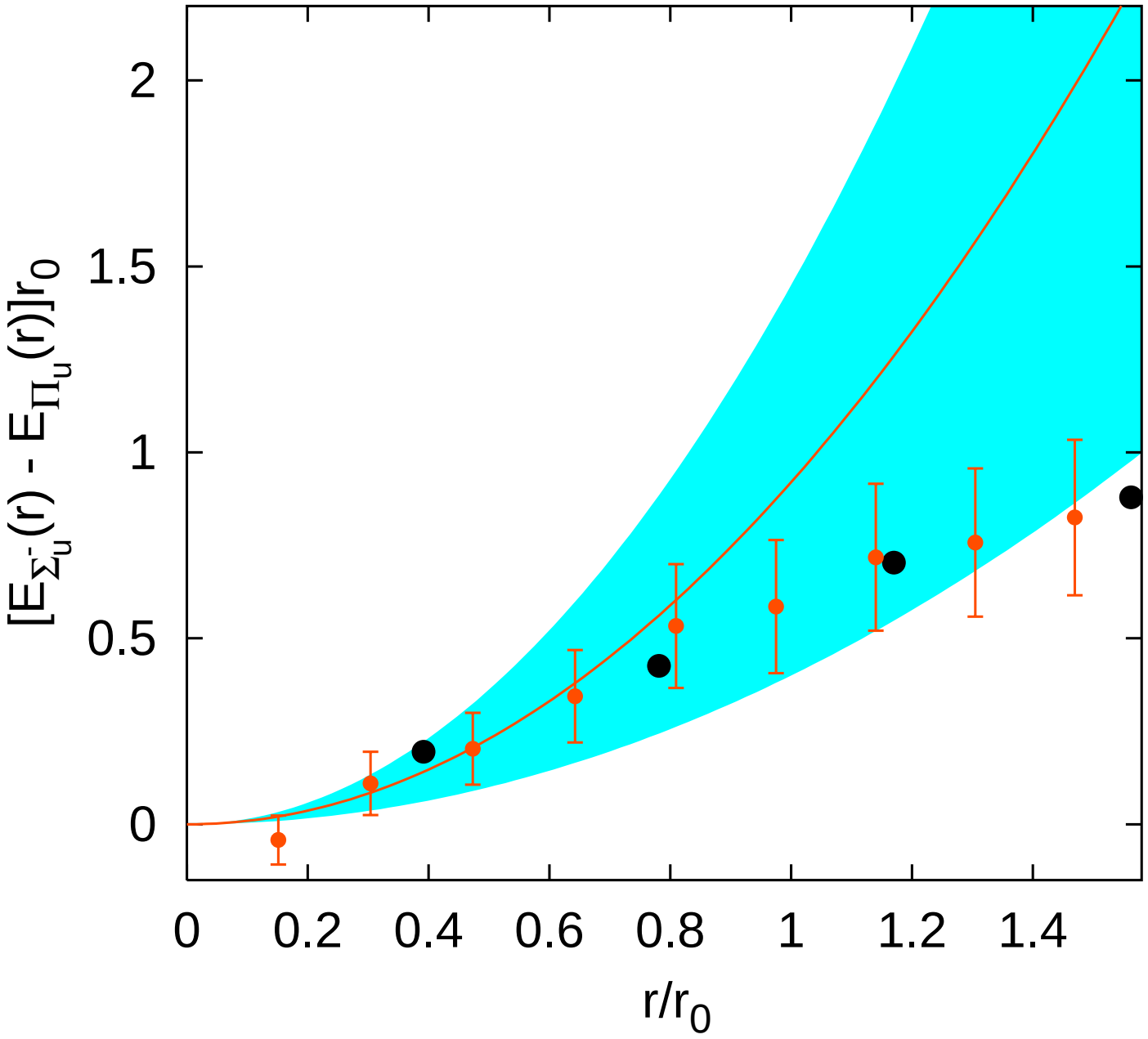

Figure 22: Splitting between the Σ_u^- and the Π_u potentials, extrapolated to the continuum limit, and the comparison with a quadratic fit to the $r \lesssim 0.5\, r_0$ data points ($r_0^{-1} \approx 0.4$ GeV). The big circles correspond to the data of Juge et al., obtained at finite lattice spacing $a_\sigma \approx 0.39\, r_0$. The errors in this case are smaller than the symbols. Bali-Pineda 2004.